Designing Self-Airy Shells with Unreinforced Boundaries

Yu-Chou Chiang[a,*], Hui Wang[b], Xinye Li[c], Helmut Pottmann[d]

[a] *Department of Civil Engineering, National Chung Hsing University, Taiwan*
[b] *School of Mathematics and Stasitics, Xi'an Jiaotong University, P.R. China*
[c] *College of Civil Engineering, Tongji University, P.R. China*
[d] *Institute of Discrete Mathematics and Geometry, Vienna University of Technology, Austria*

Abstract

A self-Airy membrane shell is a special type of shell structure whose shape coincides with the shell's Airy stress surface. It provides the convenient property that any polyhedral discretization of such a surface will automatically generate a mesh in funicular equilibrium. A self-Airy shell designed for a uniform vertical load would simply have a constant *isotropic* Gaussian curvature. However, a challenge in implementing a self-Airy shell in architecture is the lack of a design method, especially in designing unreinforced boundaries. Those are singular planar curves, where the two principal curvatures approach 0 and ∞ individually. This paper presents methods for designing unreinforced boundaries of self-Airy shells, including both smooth and discrete methods. These methods work for both positively and negatively curved surfaces. The proposed methods work linearly without iteration. The preliminary results show that the seemingly very restrictive conditions admit a variety of non-trivial surfaces.

Keywords: shell structure, Airy stress function, discrete differential geometry, architectural geometry, form-finding

1. Introduction

For visual simplicity, an elegant structure tends to have maximum agreement between its form and its internal forces. This paper discusses the agreement between the shell structure's form and the underlying Airy stress function, which encodes the stress tensor field [1, 2, 3]. When the shapes of a shell and its Airy stress function coincide, it is called a *self-Airy* shell [4] (Fig. 1).

In designing curved surface structures (e.g., masonry vaults, concrete shells, steel-glass grid-shells), designers can choose different degrees of agreement between the form and forces. Any misalignment of form and forces will result in additional structural elements for reinforcement, which reduces architectural appealing. For instance, an arbitrarily designed vault would require boundary walls for support and an arbitrarily designed shell would require boundary beams for reinforcement [1]. To get rid of the cumbersome walls or beams, designers should align the stress flow with the boundary. Heinz Isler developed the design technique by hanging clothes and nets to *form-find* the desired shape that is free from reinforcing beams [5]. As a result, the form-found shells can fully expose the thinness of concrete shells (see Fig. 2).

Designers can also ask for the alignment of the orientations of principal stress and principal curvature; such a surface can easily be built with CNC-cut planar quadrilateral panels without the need of diagonal bracing [6].

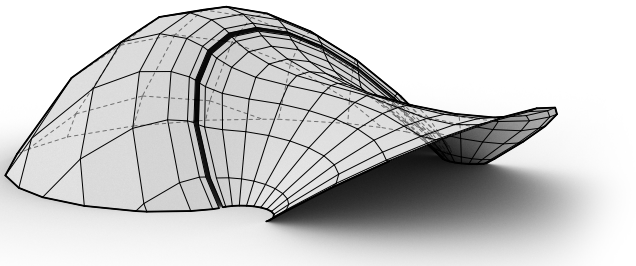

Figure 1: Two self-Airy surfaces meet at the same unreinforced boundary. The surface on the left side of the narrow skylight is positively curved, meanwhile the right-hand side is negatively curved.

This paper is asking for even more alignment: curvature and stress have not only the same principal orientation but also magnitudes. Or, more precisely, the Airy stress function and the shell have the same shape. Thus, any polyhedral surface discretizing the shape is also a polyhedral discretization on the Airy stress function. Therefore, the resultant mesh is funicular (i.e., structural equilibrium only relies on axial forces of the mesh edges) and has planar faces (Fig. 1).

When the load per horizontal area is constant, a self-Airy shell has a constant *isotropic* Gaussian curvature (^{i}K). This surface is the basis for the design of all other *isotropic* linear Weingarten surfaces [7], which are the shells that have the *isotropic* principal stress and curvature aligned [8, 9]. Strubecker [10] has provided great insight into constant *isotropic* Gaussian curvature surfaces. This paper extends Strubecker's method to discrete meshes and includes singular points to create more complex yet interesting designs for such surfaces.

* Present address: Department of Architecture, National Cheng Kung University, Taiwan. Postal address: 1 Dasyue Road, East District, Tainan 701401, Taiwan. E-mail address: Chiang.YuChou@gmail.com

Figure 2: A form-found shell with unreinforced boundaries by Isler (top) and a hyperbolic paraboloid shell with boundary beams (bottom) [Sources: Chriusha/CC-BY-SA-3.0; Linda Spashett/CC-BY-3.0]

1.1. Related research

As Aish et al. [11] suggest, form-finding is the process of seeking "good" shapes. There are various ways to quantify what constitutes a good shape, one of which is based on structural equilibrium. Pottmann et al. [12] refer to this approach as "statics-aware design". Notable research in this area includes dynamic relaxation [13], the force density method [14], trust network analysis [15]. Most of these studies focus on utilizing membrane stresses to balance the external loads [16, 17, 18, 19, 20], while some also incorporate transverse shears and bending moments [21, 22]. Some studies express the statics geometrically, in 2D [15, 18] or in 3D [23, 24, 25]

Another way to quantify good shapes is based on manufacturability, referred to as "fabrication-aware design" [12], considering how easily the components can be fabricated. Since the fabrication of free-form surfaces often relies on industrially mass-produced planar panels, it is practical to discretize free-form surfaces into planar components, including surfaces consisting of planar quadrilaterals [26, 27, 28, 29] or even with planar parameter lines [29].

Geometry plays a crucial role not only in discretizing curved surfaces into polyhedral forms but also in the statics. Minimal surfaces, for example, resemble soap films and can be elegantly realized as tensile structures [11]. Constant mean curvature surfaces and constant Gaussian curvature surfaces can be constructed as funicular structures using planar quadrilaterals and torsion-free nodes [30, 31]. These surfaces belong to the family of "linear Weingarten surfaces", which have the constant weighted sum of mean and Gaussian curvatures. Remarkably, both scaled and offset copies of a linear Weingarten surface also remain within the same surface family [7].

For shallow shells under vertical loads, *isotropic* geometry offers valuable insights (see § 2.3). A shell structure shaped as an *isotropic* linear Weingarten surface possesses an Airy stress function whose *isotropic* principal orientations of curvatures align with those of the surface [8, 9]. This alignment means that an *isotropic* principal mesh discretization of such a surface is automatically funicular (a desirable equilibrium condition [32]) without the need for diagonal bracing when subjected to a uniform vertical load. Pellis and Pottmann [6] also explored the alignment of principal stress and curvature orientations, although their work was situated in Euclidean space rather than *isotropic* space.

Millar et al. [4] as well as Chiang [25, 33] had tried to merge the shape of the shell and the Airy stress function even further. They had sought the shells that have the same shape as their Airy stress function. They call such cases "self-Airy" shells. The self-Airy shells presented in Millar et al. [4] are all well supported and no unsupported boundaries are left. The cases in Chiang [33] contain unsupported and unreinforced boundaries. However, the numerical cases were solved by solving the bilinear Pucher's equation iteratively. Furthermore, the results were limited to positively curved surfaces.

Under a uniform vertical load, a self-Airy shell is a constant *isotropic* Gaussian curvature surface. Strubecker [10, pp.554–559] extensively discussed how to generate a smooth *isotropic* Gaussian curvature surface from a parameterized analytical curve. Strubecker's insights serve as an important building block of this paper. However, his method is limited to the surface of a regular parameter net.

One may connect regular parameter nets to form a semi-regular net. Shearman and Venkataramani [34] noted that, for negatively curved constant Gaussian curvature surfaces with a semi-regular asymptotic net, the asymptotic curves will be only C^1-smooth across the boundaries between the regular patches. Meanwhile, at the junctions of the borders, one can observe the singular or "branch point" of the asymptotic net. Their insights also benefit this paper greatly when we look into how to deliver more interesting self-Airy meshes.

1.2. Contributions and overview

The structure of the paper and its contributions can be summarized as follows:

- We review the theories of membrane shells, self-Airy surfaces, metric duality, and constant *isotropic* Gaussian curvature surfaces (§ 2).

- Subsequently, smooth constant *isotropic* Gaussian curvature surfaces are constructed from arbitrary unreinforced boundaries (§ 3).
- We show how to construct discrete constant *isotropic* Gaussian curvature meshes in a set of linear processes without iterative computation (§ 4).
- Regular quadrilateral meshes are combined into semi-regular ones, which have much more architectural design freedom (§ 5).
- We present some architectural designs with these meshes (§ 6), conclude the current findings, and set out some future research directions (§ 7).

2. Theories of self-Airy shells and constant *isotropic* Gaussian curvature surfaces

In this section, we first review the classical theories of general shell structures (§ 2.1). Readers who are already familiar with mechanics of shells can proceed to § 2.2 for the discussion on self-Airy shells, § 2.3 for a brief introduction to *isotropic* geometry, or § 2.4 for Maxwell's duality.

2.1. General membrane shells

Shells that carry load only with membrane stresses (i.e., tension and compression) without bending moments are called *membrane shells*. In the absence of body forces, horizontal components of stress per unit horizontal length N_{ij} ($i, j \in \{x, y\}$) of a membrane shell in an equilibrium state can be represented by second derivatives of a smooth Airy stress function $F(x, y)$ [35, 36]:

$$\begin{bmatrix} N_{xx} & N_{xy} \\ N_{xy} & N_{yy} \end{bmatrix} = \begin{bmatrix} F_{,yy} & -F_{,xy} \\ -F_{,xy} & F_{,xx} \end{bmatrix}, \tag{1}$$

where the partial derivatives are expressed by the subscripts such as $[\cdot]_{,ij} = (\partial^2/\partial i \partial j)[\cdot]$. This expression automatically satisfies the equilibrium equations of the horizontal directions: $N_{xx,x} + N_{xy,y} = 0$, $N_{xy,x} + N_{yy,y} = 0$ [35, 37, 38].

The equilibrium in the vertical direction is governed by

$$Z_{,xx}\, N_{xx} + 2\, Z_{,xy}\, N_{xy} + Z_{,yy}\, N_{yy} = -p_z,$$

where $Z(x, y)$ is the elevation of the shell and p_z is the vertical load per horizontal unit area.

Governing equation. By expression (1), the vertical equilibrium becomes Pucher's equation [37, 38]:

$$Z_{,xx}\, F_{,yy} - 2\, Z_{,xy}\, F_{,xy} + Z_{,yy}\, F_{,xx} = -p_z. \tag{2}$$

This single equation (2) governs the equilibrium of all three directions. It also suggests that the vertical load p_z equals the bilinear form of the two scalar functions: the shape $Z(x, y)$ and the Airy stress function $F(x, y)$.

Conditions for unreinforced boundaries. When a segment of a shell's edge is free from structural support, structural engineers conventionally call it a "free edge". In this paper, we call it an *unreinforced boundary*, provided that the term "edge" will be confused with the border lines between faces of a polyhedral surface. At such a boundary, there should be no normal stress transmitting across the boundary nor shear stress acting along the edge. These two conditions can be expressed as

$$N_{nn} = F_{,tt} = 0, \qquad N_{nt} = -F_{,nt} = 0, \tag{3}$$

where the subscripts $[\cdot]_{,tt}$ and $[\cdot]_{,nt}$ denote the second-order directional derivatives, n and t are normal and tangential vectors of the boundary. These conditions require the stress function $F(x, y)$ to be tangential to a plane at the boundary [1, 39].

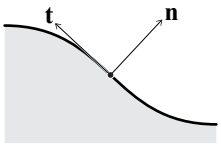

2.2. Self-Airy membrane shells

Governing equation. When the shape of a shell coincides with its Airy stress function: $F(x, y) = F_0 \cdot Z(x, y)$, Pucher's equation (2) turns into

$$Z_{,xx}\, Z_{,yy} - Z_{,xy}^2 = -\frac{p_z}{2F_0}. \tag{4}$$

The left-hand side of equation (4) is the determinant of the Hessian matrix of the shape $Z(x, y)$. This determinant is also the *isotropic* Gaussian curvature of the shell [40, 41]. When the vertical load per horizontal area p_z is constant, the self-Airy surface has a constant *isotropic* Gaussian curvature.

Similar to a smooth Airy stress function that can be discretized into a polyhedral surface [42], the self-Airy surfaces can also be discretized [4, 25]. The resulting surfaces have planar faces and are all funicular nets at the same time. This is a desired feature because the need for diagonal bracing of such a surface is minimized, which can improve the visual clarity of the structure.

Constant p_z. This paper remains within the assumption of constant p_z, although a uniform thickness shell should have the realistic gravitational load $p_z \propto \sqrt{1 + s^2}$, where $s = \sqrt{Z_{,x}^2 + Z_{,y}^2}$ is the slope. This suggests that where the slope is 20%, the realistic gravitational load is approximately 2% higher than the simplified assumption. In engineering practices, an approximate error below 5% is acceptable. More importantly, gravitational load is just one of many factors to consider when approving a structure. Therefore, the assumption of a constant p_z is largely valid, especially for a conceptual design phase.

Conditions for unreinforced boundaries. For a self-Airy shell, the unreinforced boundaries are planar and singular. Conditions (3) apply to its shape, therefor when a point in a self-Airy shell approaches an unreinforced boundary,

$$Z_{,tt} \to 0, \qquad Z_{,nt} \to 0. \tag{5a}$$

Since equation (4) should be satisfied, $Z_{,nn}$ must approach infinity:

$$Z_{,nn} \to \infty. \tag{5b}$$

By (5a), we can infer that the unreinforced boundaries of a self-Airy shell must be planar. By (5b), we know that such boundaries are also singular. Taken together, the boundary conditions (5) require that an unreinforced boundary be tangent to a plane and possess one infinite principal curvature.

2.3. Isotropic geometry

The right geometric framework for studying the Airy stress surface is so-called *isotropic geometry*.

Be aware that the term *isotropic* here has a different meaning from "having the same properties in all directions". In classical geometry, it refers to lines on which the length measurement degenerates. Those are not real in Euclidean geometry, but other geometries may contain real *isotropic* lines. An example is provided by so-called *isotropic* geometry, which has first been set out by Strubecker [43, 44, 45, 46], who has been the first to realize that the graph of the Airy stress function should be studied within *isotropic* geometry [47], as explained below.

Let us consider a body in the xy-plane, in equilibrium with forces only applied at its boundary. Then, its associated Airy stress function $F(x, y)$ is only determined up to the addition of a linear function, since that does not influence the Hessian $\mathbf{H}(F)$ of F, which is the adjoint of the stress tensor and contains the essential mechanical characteristics. Since the mechanical characteristics of the 2D stress state should not depend on the Cartesian system chosen in the plane, a geometric study of the Airy stress surface $z = F(x, y)$ should be based on concepts that are invariant under the following group G_6 of affine transformations:

$$\begin{aligned} x' &= a + x\cos\theta - y\sin\theta, \\ y' &= b + x\sin\theta + y\cos\theta, \\ z' &= c + c_x x + c_y y + z, \end{aligned} \tag{6}$$

where a, b, c are constants of translation and c_x, c_y, θ are constants of *isotropic* rotation. These are the *isotropic* motions, and the geometry based on that group is known as *isotropic* geometry. Geometry in *isotropic* 3-space I^3 has been developed by K. Strubecker in a series of papers [43, 44, 45, 46, 10], which led to many further contributions. Most of them are contained in the monograph by Sachs [41]. Here, we just outline some basic facts on self-Airy surfaces that are useful for the application in structural design. We also add a few remarks to provide a deeper insight into the presented constructions.

Maxwell paraboloid and curvatures. Maxwell already used the following rotational paraboloid Σ in his studies on reciprocal diagrams [48, 49, 50]:

$$\Sigma: \; z = \frac{1}{2}\left(x^2 + y^2\right). \tag{7}$$

In *isotropic* geometry, it plays the role of a unit sphere. The *isotropic* surface theory uses the following counterpart to the Gauss map and shape operator of Euclidean surface theory: Given a surface S, the *isotropic* Gauss map γ maps a point $p \in S$ to a point $\gamma(p) \in \Sigma$ in such a way that the tangent planes of S at p and of Σ at $\gamma(p)$ are parallel. The derivative of this map is the *isotropic* shape operator, from which curvatures are deduced as in the Euclidean case. In particular, its determinant is the *isotropic* Gauss curvature ${}^{\mathrm{i}}K$. If the surface S is given in the form $z = f(x, y)$, one has

$${}^{\mathrm{i}}K = f_{,xx} \cdot f_{,yy} - f_{,xy}^2, \tag{8}$$

showing that the self-Airy surfaces discussed above have constant *isotropic* Gaussian curvature [4].

One can also relate the *isotropic* Gaussian curvature ${}^{\mathrm{i}}K$ with its Euclidean counterpart ${}^{\mathrm{E}}K$:

$${}^{\mathrm{i}}K = {}^{\mathrm{E}}n_z^{-4} \cdot {}^{\mathrm{E}}K = (1 + s^2)^2 \cdot {}^{\mathrm{E}}K, \tag{9}$$

where ${}^{\mathrm{E}}n_z$ is the z-component of the normalized Euclidean normal vector, $s = \sqrt{Z_{,x}^2 + Z_{,y}^2}$ is the slope (see e.g., [51], p. 36). This suggests that when the slope is 0%, *isotropic* Gaussian curvature ${}^{\mathrm{i}}K$ has the same value as its Euclidean counterpart ${}^{\mathrm{E}}K$. When the slope is 20%, the value of ${}^{\mathrm{i}}K$ is approximately 8.2% higher than ${}^{\mathrm{E}}K$.

2.4. Maxwell polarity and metric duality

Maxwell also used Σ via its polarity. It is a projective duality δ that maps a point $\Xi = (\xi, \eta, \zeta)$ to a plane

$$\delta(\Xi) = P : z + \zeta = \xi x + \eta y$$

and vice versa: $\delta(P) = \Xi$. For geometric interpretations of this polarity, readers are referred to Crapo and Whiteley [52] and Konstantatou et al. [53].

This polarity realizes a *metric duality in isotropic space* I^3, which has no counterpart in Euclidean geometry. Since *isotropic* motions appear in the top view as Euclidean 2D motions, the *isotropic* distance of a pair of points $\Xi_i = (\xi_i, \eta_i, \zeta_i)$, $i = 1, 2$ is naturally defined as Euclidean distance in the top view, $d = \sqrt{(\xi_1 - \xi_2)^2 + (\eta_1 - \eta_2)^2}$. Applying metric duality to these pair of points, one obtains two planes $\delta(\Xi_i) : \; z = \xi_i x + \eta_i y - \zeta_i$, whose *isotropic* angle equals d. Thus, metric duality turns the distance of two points into the angle of the image planes, and vice versa.

Metric duality maps a surface S (as a set of contact elements, i.e., points and tangent planes) to a surface $\delta(S)$ (as a set of contact elements, i.e., tangent planes and their contact points). A contact element of S with *isotropic* Gauss curvature ${}^{\mathrm{i}}K$ corresponds to a contact element of $\delta(S)$ with Gauss curvature $1/{}^{\mathrm{i}}K$. Hence, self-Airy surfaces as those with ${}^{\mathrm{i}}K = {}^{\mathrm{i}}K_0 = const.$ correspond in metric duality to self-Airy surfaces with ${}^{\mathrm{i}}K = 1/{}^{\mathrm{i}}K_0$. As in any projective duality, asymptotic tangents correspond to asymptotic tangents. The asymptotic curves of constant torsion $\pm\sqrt{-{}^{\mathrm{i}}K}$ get mapped to asymptotic curves of constant torsion $\pm 1/\sqrt{-{}^{\mathrm{i}}K}$, in agreement with the constant Gauss curvature $1/{}^{\mathrm{i}}K$.

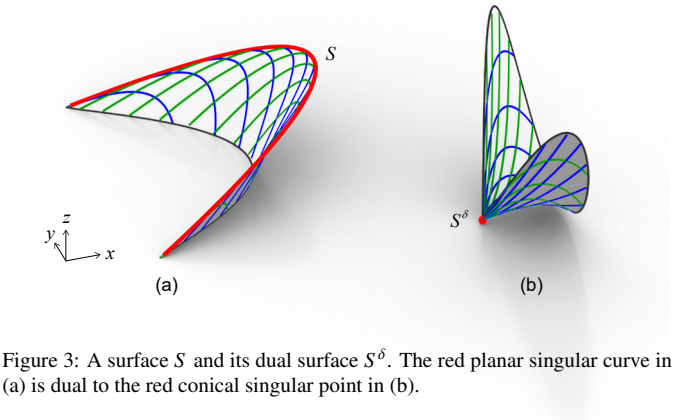

Figure 3: A surface S and its dual surface S^δ. The red planar singular curve in (a) is dual to the red conical singular point in (b).

Under metric duality, a planar singular curve (unreinforced boundary) corresponds to a cone singularity and vice versa (fig. 3).

Remarkably, *metric duality* δ maps a plane T_p to a point $\delta(T_p)$ which has the same top view as the image of the plane under the *isotropic* Gauss map γ. Let $\delta(T_pS)$ denote the image of a tangent plane T_pS with a tangency point $p \in S$ on the surface S under the *metric duality* δ. Let $\gamma(p)$ denotes the image of the point p under the *isotropic* Gauss image γ. The two points $\delta(T_pS)$ and $\gamma(p)$ are contained in the same vertical line. Since the duality δ shares the same top view as the Gauss image γ, we will extensively use duality in the following sections. The readers are advised to bear in mind that the distances in the dual surface correspond to angles in the primal surface.

3. Simple construction of constant ${}^{\mathrm{i}}K$ surfaces

In this section, we present a simple introduction to explicit construction methods for self-Airy surfaces with constant vertical loads. In the classical geometric literature, they go back to Darboux's solution of the Monge Ampere equation, but the deeper geometric roots of this construction have been uncovered by K. Strubecker in a series of papers that study them within *isotropic* geometry [44, 45, 46, 10]. In *isotropic* space, these surfaces possess constant Gaussian curvature.

While we are also addressing the general construction of self-Airy surfaces, we emphasize those having an unreinforced boundary, i.e., possess a planar singular curve. Their construction does not require any knowledge of *isotropic* geometry. Our focus is on proposing discrete versions (§ 4) that are not found in the classical literature.

3.1. Strubecker's construction

In a paper on relations between the so-called paratactic map and the theory of closed planar convex curves, Strubecker [10] presented the following geometric construction of surfaces which solve equation (4) with constant p_z, and thus constant ${}^{\mathrm{i}}K$, and possess a given planar curve $c(t) = (c_x(t), c_y(t), 0)$ as a singular curve. The restriction of this curve onto the plane $z = 0$ is easily removed later by adding a linear function to the solution, which is equivalent to an affine shearing in z-direction (x,y,z) $\mapsto (x, y, z + ax + by + d)$.

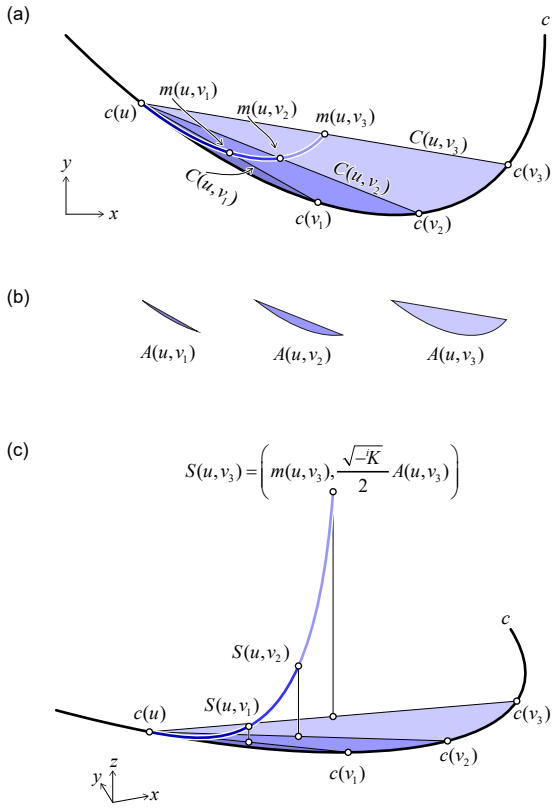

Figure 4: Strubecker's construction of an isoparametric curve of the self-Airy surface with a given curve $c(t)$ in the plane $z = 0$ as the singular curve. (a) The top view of the self-Airy surface $S(u, v)$ is the midpoints of $c(u)$ and $c(v)$. (b-c) The height of the surface $S(u, v)$ is proportional to the area $A(u, v)$ bounded by the curve c and the line segment $c(u)c(v)$. Note that the areas shown in (b) have been scaled down for brevity.

One picks any two points on the planar curve c, say $c(u)$ and $c(v)$ and considers the midpoint $m(u, v) = [c(u) + c(v)]/2$ of the straight line segment $C(u, v)$ with these points ($c(u)$ and $c(v)$) as end points. Then, one takes z-coordinate at $m(u, v)$ proportional to the oriented area $A(u, v)$ of the segment which is cut off by $C(u, v)$ from c (see Fig. 4). With varying choices of the parameters (u, v) one obtains the announced solution surface $S(u, v) = (m(u, v), \sqrt{-{}^{\mathrm{i}}K}/2 \cdot A(u, v))$ of equation (4). Analytically, we do not obtain it in explicit form $z = Z(x, y)$, but in a parametric representation:

$$S(u,v) = \left(\frac{1}{2}\big[c_x(u) + c_x(v)\big],\ \frac{1}{2}\big[c_y(u) + c_y(v)\big], \right.$$
$$\frac{\sqrt{-{}^{\mathrm{i}}K}}{4} \Big\{ \int_u^v \big[c_x(t)\dot{c}_y(t) - \dot{c}_x(t)c_y(t)\big]\, dt$$
$$\left. - \big[c_x(u)c_y(v) - c_x(v)c_y(u)\big] \Big\} \right), \qquad (10)$$

where dots above the functions indicate derivatives. The formula can be applied to any choice of u and v. In all cases, $A(u, v)$ is the oriented area of the domain swept out by the line segment $Oc(t)$ for $t \in [u, v]$ (O being the origin) minus the ori-

ented area of the triangle $Oc(u)c(v)$ (fig. 5).

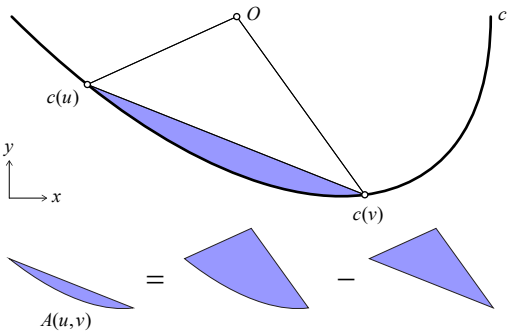

Figure 5: The calculation of area $A(u, v)$

It is remarkable that Strubecker's simple construction yields all solutions:

Theorem 1. *Application of affine maps of the form* $(x, y, z) \mapsto (x, y, d + ax + by + ez)$ *to surfaces* $S(u, v)$ *in equation (10) yields all possible negatively curved self-Airy surfaces with constant vertical loads and an unreinforced boundary curve c.*

Proof. We only sketch the proof, since it would require more details on the paratactic map that underlies the construction. The paratactic map takes surface elements (points $X = (x_1, x_2, x_3)$ plus their tangent planes $T(X) : z = px + qy + r$, with $x_3 = px_1 + qx_2 + r$) as input and maps them to two points $X_l = (x_1 + p, x_2 - q, 0)$ and $X_r = (x_1 - q, x_2 + p, 0)$ in the plane $z = 0$. X_l and X_r are called left and right image points. A general surface has a left and right image domain that are related by an area-preserving map. Exactly for a surface that solves equation (4) with constant right-hand side -1, the left and right images are curves. Exactly if we put the unreinforced boundary into the plane $z = 0$, these curves agree and constitute a singular curve c of the surface. This is the case described by equation (10). To get another constant on the right-hand side of (4), we multiply the z-coordinate with a factor e. To move the singular curve c to a more general position, we add a linear function $ax + by + d$ to the z-coordinates. □

Duality of Strubecker's construction. As stated in § 2.4, the duality is convenient for us to discuss the curvature of the surfaces since the top view of the image under duality is the same as the top view of the image of the Gauss map.

The slopes of the tangent plane T_pS for a tangency point $p = S(u, v)$ can be defined via the cross product of the first derivatives $S_{,u}$ and $S_{,v}$, which are included in Appendix A (eq. A.6). Let S^δ denote the dual of S, so that $S^\delta = \delta(S)$. We can express the dual surface in a parametric representation

$$S^\delta(u,v) = \sqrt{-{}^{\mathrm{i}}K} \cdot \Big(\frac{c_y(u) - c_y(v)}{2}, \ \frac{-c_x(u) + c_x(v)}{2}, \ \frac{1}{4}\Big\{ - \int_u^v \big[c_x(t)\dot{c}_y(t) - \dot{c}_x(t)c_y(t)\big]\, dt - \big[c_x(u)c_y(v) - c_x(v)c_y(u)\big]\Big\}\Big). \quad (11)$$

3.2. Negatively curved constant ${}^{\mathrm{i}}K$ surfaces

Strubecker's construction (10) is readily applied to negatively curved surfaces where ${}^{\mathrm{i}}K < 0$, therefore the z-coordinate stays as a real number. Let us consider cases with ${}^{\mathrm{i}}K = -1$.

Example 2. *A simple example is provided by a parabola* $(c_x, c_y) = (-t^2, t)$*, which yields the primal and dual surfaces (fig. 6 b-c):*

$$S(u,v) = \Big(-\frac{u^2+v^2}{2}, \ \frac{u+v}{2}, \ -\frac{u^3-v^3}{12} + \frac{u^2v - uv^2}{4}\Big),$$
$$S^\delta(u,v) = \Big(\ \frac{u-v}{2}, \ \frac{u^2-v^2}{2}, \ \frac{u^3-v^3}{12} + \frac{u^2v - uv^2}{4}\Big).$$

Example 3. *We can also take curve c as an ellipse* $(c_x, c_y) = (a\cos t, b\sin t)$*, yielding primal and dual surfaces (fig. 6 d-e):*

$$S(u,v) = \Big(\frac{a}{2}[\cos u + \cos v], \ \frac{b}{2}[\sin u + \sin v], \ \frac{ab}{4}[-u + v + \sin(u-v)]\Big),$$
$$S^\delta(u,v) = \Big(\frac{b}{2}[\sin u - \sin v], \ \frac{a}{2}[-\cos u + \cos v], \ \frac{ab}{4}[u - v + \sin(u-v)]\Big).$$

This surface is an affine image of a rotational surface that is obtained for $a = b$. It is a special instance of the following fact, which follows from (10): Application of an affine map $(x, y, z) \mapsto (ax, by, abz)$ maps a self-Airy surface to another self-Airy surface.

3.3. Positively curved constant ${}^{\mathrm{i}}K$ surfaces

Self-Airy surfaces of positive curvature can be obtained analogously to those with negative curvature. However, since their asymptotic curves are not real, we must use the complex extension [44]. When ${}^{\mathrm{i}}K > 0$, real parameters u, v leave Strubecker's construction (10) a non-real surface. However, inserting conjugate complex parameters $u, v = \overline{u}$ via

$$\begin{bmatrix} u \\ v \end{bmatrix} = \frac{1}{2}\begin{bmatrix} 1+i & 1-i \\ 1-i & 1+i \end{bmatrix}\begin{bmatrix} r \\ s \end{bmatrix} \Leftrightarrow \begin{bmatrix} r \\ s \end{bmatrix} = \frac{1}{2}\begin{bmatrix} 1-i & 1+i \\ 1+i & 1-i \end{bmatrix}\begin{bmatrix} u \\ v \end{bmatrix}, \quad (12)$$

we obtain a real surface $R(r, s)$ for real r, s. We assume here that the involved functions c_i ($i \in \{x, y\}$) are real analytic: $c_i(\overline{u}) = \overline{c_i(u)}$. Since the parameters are conjugate $u, v = \overline{u}$, we have the complex extension satisfies $c_i(u) + c_i(\overline{u}) = c_i(u) + \overline{c_i(u)} = 2\,\mathrm{Re}(c_i(u))$. Therefore, the first two coordinates of $R(r, s)$ are real. The third coordinate is of the type $i\{g(u) - g(\overline{u})\} = i\{g(u) - \overline{g(u)}\} = i\{2i \cdot \mathrm{Im}(g(u))\} = -2\,\mathrm{Im}(g(u))$, where $g(u)$ represents the results of algebraic and analytic operations of c_i. Hence, all coordinates of $R(r, s)$ are real.

After affirming the surface $R(r, s)$ is real when ${}^{\mathrm{i}}K > 0$. Let us consider the cases with simply ${}^{\mathrm{i}}K = 1$.

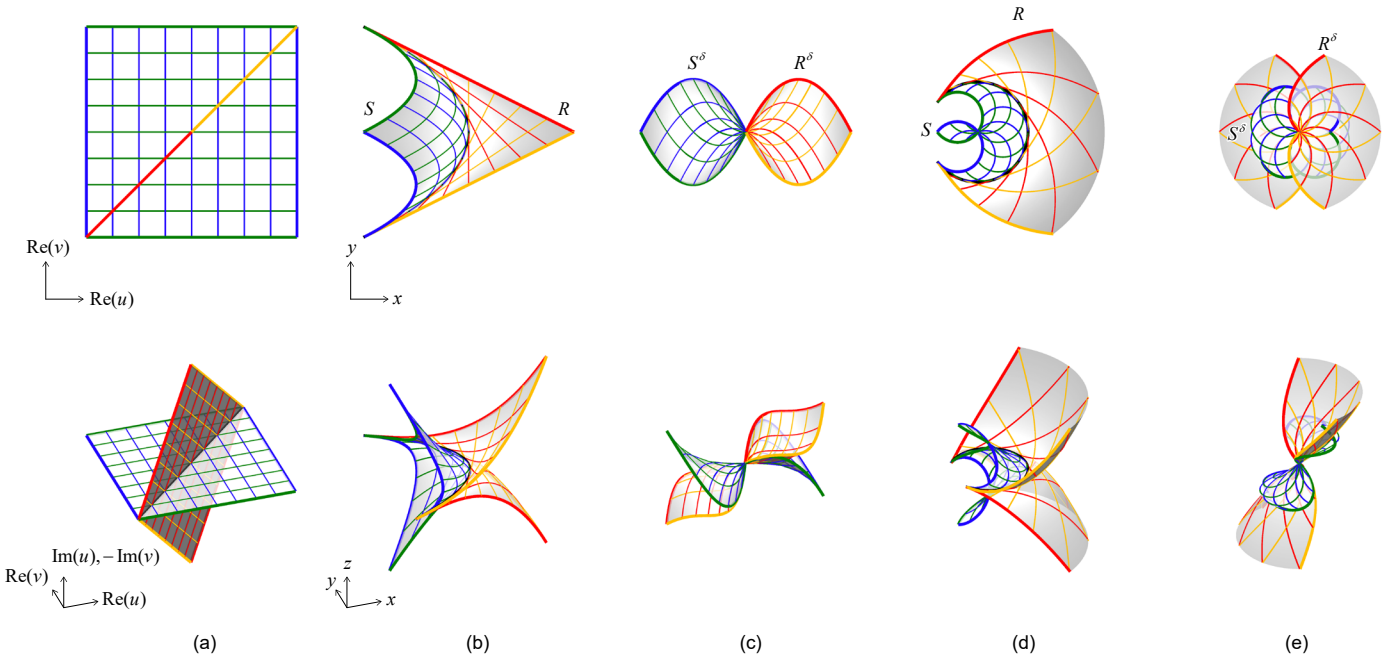

Figure 6: Self-Airy surfaces with a parabola (b) or a circle (a degenerate ellipse) (d) as the singular curve and their dual surfaces, resp. (c) & (e). The real parameter net (blue and green) is associated with the negatively curved surfaces (see Examples 2 and 3). The blue and green iso-parameter lines are asymptotic curves and form a translation net in the top view. The complex parameter net (red and yellow) is associated with the positively curved surfaces (see Examples 4 and 5).

Example 4. *For the case of a parabola* $(c_x, c_y) = (-t^2, t)$*, we can have the primal and the dual surfaces*

$$S(u,v) = \left(-\frac{u^2+v^2}{2}, \frac{u+v}{2}, -i\frac{u^3-v^3}{12} + i\frac{u^2v-uv^2}{4}\right),$$
$$S^\delta(u,v) = \left(i\frac{u-v}{2}, i\frac{u^2-v^2}{2}, i\frac{u^3-v^3}{12} + i\frac{u^2v-uv^2}{4}\right),$$

which after the parameter change have the real parameterization (fig. 6 b-c)

$$R(r,s) = \left(-rs, \frac{r+s}{2}, -\frac{(r-s)^3}{12}\right),$$
$$R^\delta(r,s) = \left(-\frac{r-s}{2}, -\frac{(r+s)(r-s)}{2}, -\frac{(r-s)(r^2+rs+s^2)}{6}\right).$$

The surface contains the parabola for $r-s=0$. It is a singular curve, since $R_{,r} - R_{,s} = (0,0,0)$ along $r-s=0$. The surface is a translation surface, obtained by translating the parabola $(-s^2, s, 0)$ (when $r-s=0$) along the cubic $(s^2, 0, -s^3/3)$ (when $r+s=0$), which has a cusp at $r-s=0$. This surface is found in the classification of all translation surfaces with constant Gauss curvature in *isotropic* space [54].

This parameterized surface has the derivatives

$$R_{,r} = \left(-s, \frac{1}{2}, -\frac{(r-s)^2}{4}\right), \tag{13}$$
$$R_{,s} = \left(-r, \frac{1}{2}, \frac{(r-s)^2}{4}\right), \tag{14}$$
$$R_{,rs} = \left(-1, 0, \frac{r-s}{2}\right), \tag{15}$$

which suggest that the determinant $(R_{,r}, R_{,s}, R_{,rs}) = 0$, and thus the parameterization $R(r,s)$ is conjugate. This conjugacy can also be found in other positively curved examples, but we did not find it in the literature. We discuss it in greater detail in remark 8.

Example 5. *For the case of an ellipse* $c_x(t) = a\cos t, c_y(t) = b\sin t$*, yielding the surfaces*

$$S(u,v) = \left(\frac{a}{2}[\cos u + \cos v], \frac{b}{2}[\sin u + \sin v], i\frac{ab}{4}[-(u-v) + \sin(u-v)]\right),$$
$$S^\delta(u,v) = \left(i\frac{b}{2}[-\sin u + \sin v], i\frac{a}{2}[\cos u - \cos v], i\frac{ab}{4}[u-v+\sin(u-v)]\right),$$

which after the parameter change have the real parameterization

$$R(r,s) = \left(a\cos\frac{r+s}{2}\cosh\frac{r-s}{2}, b\sin\frac{r+s}{2}\cosh\frac{r-s}{2}, \frac{ab}{4}[r-s-\sinh(r-s)]\right),$$
$$R^\delta(r,s) = \left(-b\cos\frac{r+s}{2}\sinh\frac{r-s}{2}, -a\sin\frac{r+s}{2}\sinh\frac{r-s}{2}, \frac{ab}{4}[-(r-s)-\sinh(r-s)]\right).$$

The real parameterization $R(r, s)$ is also illustrated in figure 6d-e.

3.4. Remarks on Strubecker's construction

We make a few observations on Strubecker's construction (10). These remarks can help us later extend Strubecker's construction to discrete curves.

Remark 6. *Strubecker's construction* (10) *gives an overlapping net in the top view for both negatively and positively curved surfaces:*

$$S_x(u, v) = S_x(v, u), \qquad S_y(u, v) = S_y(v, u), \tag{16a}$$
$$R_x(r, s) = R_x(s, r), \qquad R_y(r, s) = R_y(s, r). \tag{16b}$$

The following observations are based on the first and second derivatives of the primal surface $S(u, v)$ and the dual surface $S^\delta(u, v)$. The derivatives of $S(u, v)$ and $S^\delta(u, v)$ can help us express the derivatives of $R(r, s)$ and $R^\delta(r, s)$ via the chain rule. The useful ones are listed below:

$$R_{,r} = \frac{1+i}{2}S_{,u} + \frac{1-i}{2}S_{,v}, \tag{17a}$$
$$R_{,s} = \frac{1-i}{2}S_{,u} + \frac{1+i}{2}S_{,v}, \tag{17b}$$
$$R_{,rr} = \frac{i}{2}S_{,uu} + S_{,uv} + \frac{-i}{2}S_{,vv}, \tag{17c}$$
$$R_{,rs} = \frac{1}{2}S_{,uu} + 0 + \frac{1}{2}S_{,vv}, \tag{17d}$$
$$R_{,ss} = \frac{-i}{2}S_{,uu} + S_{,uv} + \frac{i}{2}S_{,vv}. \tag{17e}$$
$$R^\delta_{,r} = \frac{1+i}{2}S^\delta_{,u} + \frac{1-i}{2}S^\delta_{,v}, \tag{17f}$$
$$R^\delta_{,s} = \frac{1-i}{2}S^\delta_{,u} + \frac{1+i}{2}S^\delta_{,v}. \tag{17g}$$

The explicit expressions of the derivatives of $S(u, v)$ and $S^\delta(u, v)$ are included in Appendix A. Here we succinctly pointing out the crucial observations.

Remark 7. *In the top view, such a negatively curved surface has a translation net, while a positively curved one has a harmonic net.*

Proof. From Strubecker's construction (10), we can simply find that the top view has the mixed second derivative equal to zero:

$$S_{uv} = (0,\ 0,\ \dots), \tag{18a}$$

which suggests that $S(u, v)$ is a translation net in the top view. From equations (17c) and (17e), we can associate $\Delta R(r, s)$ with $S_{,uv}$:

$$\Delta R(r, s) = R_{,rr} + R_{,ss} = 2 \cdot S_{,uv} = (0,\ 0,\ \dots), \tag{18b}$$

which points out that $R(r, s)$ is harmonic in the top view. □

Remark 8. *For negatively curved surfaces, Strubecker's construction gives an asymptotic parameterization [44]. For the positively curved ones, the parameterization is conjugate.*

Proof. According to Strubecker [44], the parameterization $S(u, v)$ is asymptotic, and thus the first and second partial derivatives satisfy

$$\det(S_{,u}, S_{,v}, S_{,uu}) = \det(S_{,u}, S_{,v}, S_{,vv}) = 0, \tag{19a}$$

which can also be verified with the derivatives included in Appendix A.

By the chain rule (17), we can find

$$\det(R_{,r},\ R_{,s},\ R_{,rs}) = \frac{1}{2}\det(S_{,u},\ S_{,v},\ S_{,uu}) + \frac{1}{2}\det(S_{,u},\ S_{,v},\ S_{,vv}) = 0, \tag{19b}$$

expressing that the parameterization $R(r, s)$ is conjugate. □

Remark 9. *For the negatively curved surface, the top view of tangent vectors $S_{,u}$, $S_{,v}$ of the primal surfaces $S(u, v)$ after rotating by $\mp 90°$ and scaling up by $\sqrt{-iK}$ coincide with the top view of the corresponding tangent vectors $S^\delta_{,u}$, $S^\delta_{,v}$ of the dual surfaces $S^\delta(u, v)$:*

$$\begin{bmatrix} S^\delta_{x,u} \\ S^\delta_{y,u} \end{bmatrix} = \sqrt{-iK}\begin{bmatrix} 0 & 1 \\ -1 & 0 \end{bmatrix}\begin{bmatrix} S_{x,u} \\ S_{y,u} \end{bmatrix}, \tag{20a}$$
$$\begin{bmatrix} S^\delta_{x,v} \\ S^\delta_{y,v} \end{bmatrix} = \sqrt{-iK}\begin{bmatrix} 0 & -1 \\ 1 & 0 \end{bmatrix}\begin{bmatrix} S_{x,v} \\ S_{y,v} \end{bmatrix}. \tag{20b}$$

Equations (20) can easily be verified via equations (A.1), (A.2), (A.7) and (A.8).

Remark 10. *For the positively curved surface, the top view of tangent vectors $R_{,r}$, $R_{,s}$ of the primal surfaces $R(r, s)$ after rotating by $\mp 90°$ and scaling up by $\sqrt{iK}$ coincide with the top view of the* reverse *corresponding tangent vectors $R^\delta_{,s}$, $R^\delta_{,t}$ of the dual surfaces $R^\delta(r, s)$:*

$$\begin{bmatrix} R^\delta_{x,r} \\ R^\delta_{y,r} \end{bmatrix} = \sqrt{iK}\begin{bmatrix} 0 & 1 \\ -1 & 0 \end{bmatrix}\begin{bmatrix} R_{x,s} \\ R_{y,s} \end{bmatrix}, \tag{21a}$$
$$\begin{bmatrix} R^\delta_{x,s} \\ R^\delta_{y,s} \end{bmatrix} = \sqrt{iK}\begin{bmatrix} 0 & -1 \\ 1 & 0 \end{bmatrix}\begin{bmatrix} R_{x,r} \\ R_{y,r} \end{bmatrix}. \tag{21b}$$

Proof. From equations (17f) & (17g), we can express the x- and y-components of $R^\delta_{,r}$ and $R^\delta_{,s}$ as the linear combination of $S^\delta_{,u}$ and $S^\delta_{,v}$:

$$\begin{bmatrix} R^\delta_{x,r} \\ R^\delta_{y,r} \\ R^\delta_{x,s} \\ R^\delta_{y,s} \end{bmatrix} = \frac{1}{2}\begin{bmatrix} 1+i & 0 & 1-i & 0 \\ 0 & 1+i & 0 & 1-i \\ 1-i & 0 & 1+i & 0 \\ 0 & 1-i & 0 & 1+i \end{bmatrix}\begin{bmatrix} S^\delta_{x,u} \\ S^\delta_{y,u} \\ S^\delta_{x,v} \\ S^\delta_{y,v} \end{bmatrix}. \tag{22}$$

Equations (20) can be combined as one matrix equations:

$$\begin{bmatrix} S^\delta_{x,u} \\ S^\delta_{y,u} \\ S^\delta_{x,v} \\ S^\delta_{y,v} \end{bmatrix} = \sqrt{-iK}\begin{bmatrix} 0 & 1 & 0 & 0 \\ -1 & 0 & 0 & 0 \\ 0 & 0 & 0 & -1 \\ 0 & 0 & 1 & 0 \end{bmatrix}\begin{bmatrix} S_{x,u} \\ S_{y,u} \\ S_{x,v} \\ S_{y,v} \end{bmatrix}. \tag{23}$$

Equations (17a) & (17b) state the linear relation between the vectors $R_{,s}$, $R_{,t}$ and the vectors $S_{,u}$, $S_{,v}$. By inverting the linear

coefficient matrix, we get

$$\begin{bmatrix} S_{x,u} \\ S_{y,u} \\ S_{x,v} \\ S_{y,v} \end{bmatrix} = \frac{1}{2} \begin{bmatrix} 1-i & 0 & 1+i & 0 \\ 0 & 1-i & 0 & 1+i \\ 1+i & 0 & 1-i & 0 \\ 0 & 1+i & 0 & 1-i \end{bmatrix} \begin{bmatrix} R_{x,r} \\ R_{y,r} \\ R_{x,s} \\ R_{y,s} \end{bmatrix}. \tag{24}$$

By equations (22-24), we arrive at

$$\begin{bmatrix} R^{\delta}_{x,r} \\ R^{\delta}_{y,r} \\ R^{\delta}_{x,s} \\ R^{\delta}_{y,s} \end{bmatrix} = \sqrt{\mathrm{i}K} \begin{bmatrix} 0 & 0 & 0 & -1 \\ 0 & 0 & 1 & 0 \\ 0 & 1 & 0 & 0 \\ -1 & 0 & 0 & 0 \end{bmatrix} \begin{bmatrix} R_{x,r} \\ R_{y,r} \\ R_{x,s} \\ R_{y,s} \end{bmatrix}, \tag{25}$$

which is equivalent to equations (21). □

In the remarks 7-10, the positively curved surface $R(s,t)$ inherits the properties from the negatively curved surface $S(u,v)$ via the conjugate complex parameters (12). To be much more specific, $S_{,uv} = S_{,uv} = 0$ transforms into $R_{,ss} + R_{,tt} = R_{,ss} + R_{,tt} = 0$ (remark 7). Secondly, $\det(S_{,u}, S_{,v}, S_{,uu}) = \det(S_{,u}, S_{,v}, S_{,vv}) = 0$ transforms into $\det(R_{,r}, R_{,s}, R_{,rs}) = 0$ (remark 8). Finally, equations (20) transform into equations (21) (remarks 9 & 10).

4. Construction of constant *isotropic* Gaussian curvature meshes

The midpoint and area associated with a segmented curve are straightforward to calculate. Therefore, it would be no problem at all to apply Strubecker's construction (10) for a negatively curved mesh on any arbitrary segmented curve.

However, for a positively curved mesh, the complex extension for such a midpoint and area is anything but straightforward. There is no obvious method to a create complex extension of an arbitrary segmented curve. § 4.2 proposes a method based on the mathematical observations we have just discussed in § 3.4. Before that, we shall first discuss the easy cases: negatively curved meshes.

4.1. Negatively curved constant ${}^{\mathrm{i}}K$ meshes

We will now show that Strubecker's construction directly applies to the discrete setting (fig. 7). Instead of prescribing a smooth curve c, one prescribes a polyline c (discrete curve) with vertices $c(1), \ldots, c(N)$ in the plane $z = 0$, Now, the construction is the same as above. Pick two vertices $c(i), c(j)$, compute the midpoint $m(i,j) = (c(i) + c(j))/2$ and lift it up to the z-coordinate $A(i,j)/2$ which is equal to half the area cut off from c by the line segment $C(i,j)$ with end points $c(i), c(j)$. $A(i,j)$ is the oriented area of the closed polyline with vertices $c(i), c(i+1), \ldots, c(j), c(i)$,

$$A(i,j) = \frac{1}{2}\Bigg\{ \sum_{k=i}^{j-1} \Big[c_x(k)c_y(k+1) - c_x(k+1)c_y(k) \Big] - \Big[c_x(i)c_y(j) - c_x(j)c_y(i) \Big] \Bigg\}. \tag{26}$$

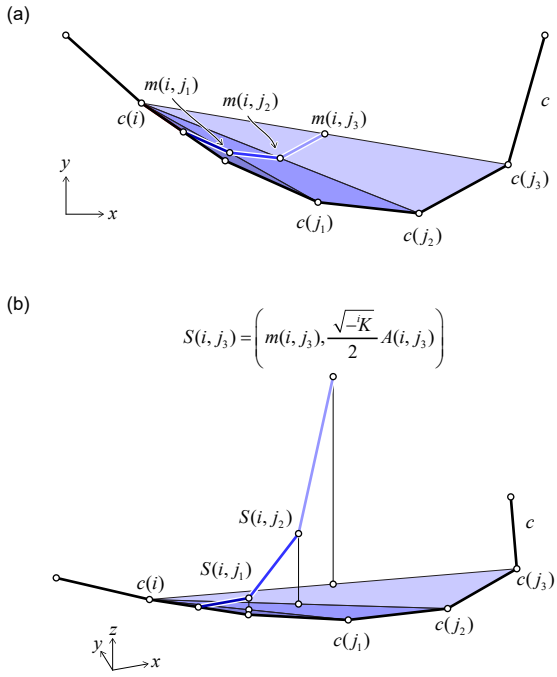

Figure 7: Construction of a self-Airy mesh with a given discrete curve c in the plane $z = 0$ as a singular curve.

The resulting point is the vertex $S(i,j)$ of a quad mesh S, which is a discrete version of a self-Airy stress surface with unreinforced boundary c. This discrete construction is not found in the literature. Remarkably, we obtain all essential properties directly in the discrete model.

Theorem 11. *The discrete version (26) of Strubecker's construction (10), illustrated in figure 7, yields quad meshes S which have planar vertex stars (edges through a vertex are coplanar) and thus are discrete asymptotic nets (A-nets). Their faces appear in the top view as parallelograms and thus the top views are translation nets. Both diagonal meshes have planar faces and are funicular. Provided that the input polyline has a constant edge length, both diagonal meshes of S have circular meshes as top views.*

Proof. We pick a segment $c(i), c(j)$, its midpoint $m(i,j)$ and corresponding mesh point $S(i,j)$ at height $A(i,j)/2$. The edges of S which emanate from $S(i,j)$ arise from the four segments shown in fig. 8. All of them have either $c(i)$ or $c(j)$ as an end point, while the other end point is a neighbor of $c(j)$ or $c(i)$, respectively. The z-coordinates of the neighboring mesh vertices $S(i,j-1), S(i+1,j), S(i,j+1), S(i-1,j)$ are obtained by either adding or subtracting half the area of a triangle with vertices $c(i), c(j)$ and one of the four points $c(i+1), c(j-1), c(j+1), c(i-1)$ as third vertex. Let $\eta(l)$ be the signed distance of $c(l)$ to the base line $c(i)\,c(j)$. Then, with $L = \|c(i) - c(j)\|$, the z-coordinate of vertex $S(i,j-1)$ equals $\sqrt{-\mathrm{i}K}/2 \cdot [A(i,j) - L\eta(j-1)/2]$, the z-coordinate of vertex $S(i+1,j)$ equals $\sqrt{-\mathrm{i}K}/2 \cdot [A(i,j) - L\eta(i+1)/2]$, and analogous

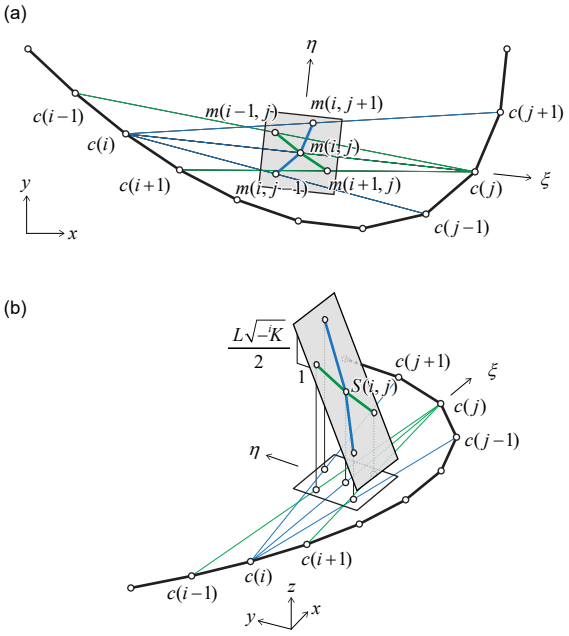

Figure 8: Illustration for the proof of Theorem 11. In the top view (a), a mesh vertex $S(i, j)$ appears as midpoint $m(i, j)$. A vertex and its neighboring points lie in the plane with slope of $L\sqrt{-{}^{\mathrm{i}}K}/2$, where L is the distance between $c(i)$ and $c(j)$. The axonometric view (b) depicts this slope.

expressions hold for the other two vertices. Introducing a local (ξ, η) frame as in Fig. 8, vertex $S(i, j)$ and its four neighbors lie in the plane with equation $z = \sqrt{-{}^{\mathrm{i}}K}/2 \cdot [A(i, j) - L\eta]$. Hence, the mesh S is a so-called A-net, a quad mesh with planar vertex stars. A-nets are a discrete counterpart to asymptotic parameterizations and well studied in discrete differential geometry [55]. The planes of vertex stars in S are face planes of the diagonal meshes. As polyhedral meshes of a self-Airy shape, the diagonal meshes are funicular. If the edges have constant length d in the top view, the direct neighbors of $m(i, j)$ lie at distance d from $m(i, j)$ and thus on a circle, showing that the top views of diagonal meshes are circular. □

Figure 9 illustrates the constructions with the same base curve, yet sampled into different polylines. They show the resulting A-nets and their diagonal meshes. Note that the discrete parameterization (set of edge lengths in the polyline) determines the shape of the diagonal nets. This is a simple way to get a variety of funicular nets via diagonal nets of A-nets.

4.2. *Positively curved constant ${}^{\mathrm{i}}K$ meshes*

Since there is no obvious method to extend an arbitrary segmented curve $c(t)$ from the real domain $t = a,\ a \in \{1, 2, \ldots, n\}$ to the complex domain $t = a + bi,\ a, b \in \{1, 2, \ldots, n\}$, Strubecker's construction (10) may not immediately be applicable to segmented curves for positively curved meshes. Instead, we can generalize the observations (Remarks 6-10) for the parameterized surface to the positively curved meshes.

A discrete parameterized surface would be a quadrilateral mesh $R(i, j),\ i, j \in \{1, 2, \ldots, n\}$. From the understanding of

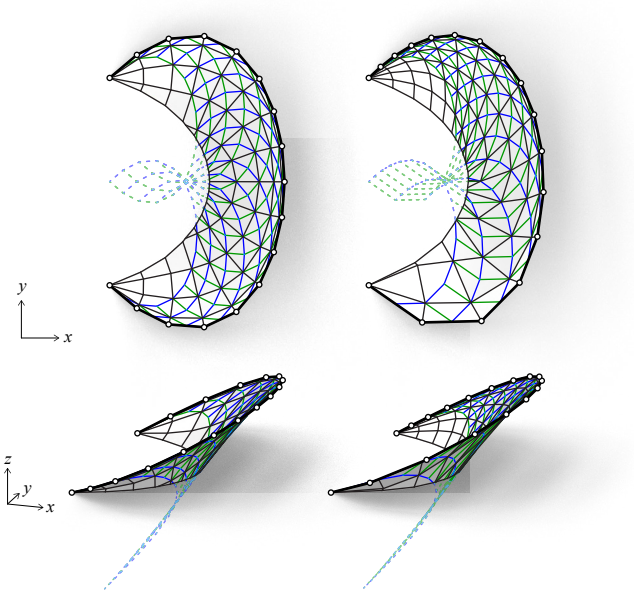

Figure 9: Two funicular meshes generated via the A-nets based on the same curve yet sampled in different intervals. (Parts of the meshes are extended and truncated to connect to the ground plane. The truncated parts are shown in dotted lines.)

the parameterized surfaces $R(r, s)$ and $R^{\delta}(r, s)$, firstly, the mesh $R(i, j)$ should be overlapping and harmonic in the top view (remarks 6 & 7). Secondly, the mesh should have planar quadrilaterals since the parameterization $R(r, s)$ is conjugate (remark 8). Thirdly, in the top view, the edges of the primal mesh $R(i, j)$ and their corresponding edges in the dual mesh $R^{\delta}(i, j)$ are orthogonal and have a constant length ratio (remark 10). By these properties, we can create a quadrilateral mesh from a segmented curve and derive the slope of each quadrilateral, then get the overall shape of the mesh.

Determine the top view of the primary mesh. The first step is to determine the top view $(R_x(i, j), R_y(i, j))$. As highlighted in remarks 6 & 7, the top view of Strubecker's construction should be overlapping $(R_x(r, s) = R_x(s, r),\ R_y(r, s) = R_y(s, r))$ and harmonic. When discretized, we can interpret the first condition as the mesh is folded along the singular curve $(i = j)$:

$$R_x(i, j) = R_x(j, i), \qquad R_y(i, j) = R_y(j, i). \tag{27a}$$

Additionally, the vertex $R(i, j)$ should sit at the barycenter of the four adjacent vertices in the top view:

$$R_x(i, j) = \frac{1}{4}\Big[R_x(i+1, j) + R_x(i-1, j) + R_x(i, j+1) + R_x(i, j-1)\Big], \tag{27b}$$

$$R_y(i, j) = \frac{1}{4}\Big[R_y(i+1, j) + R_y(i-1, j) + R_y(i, j+1) + R_y(i, j-1)\Big]. \tag{27c}$$

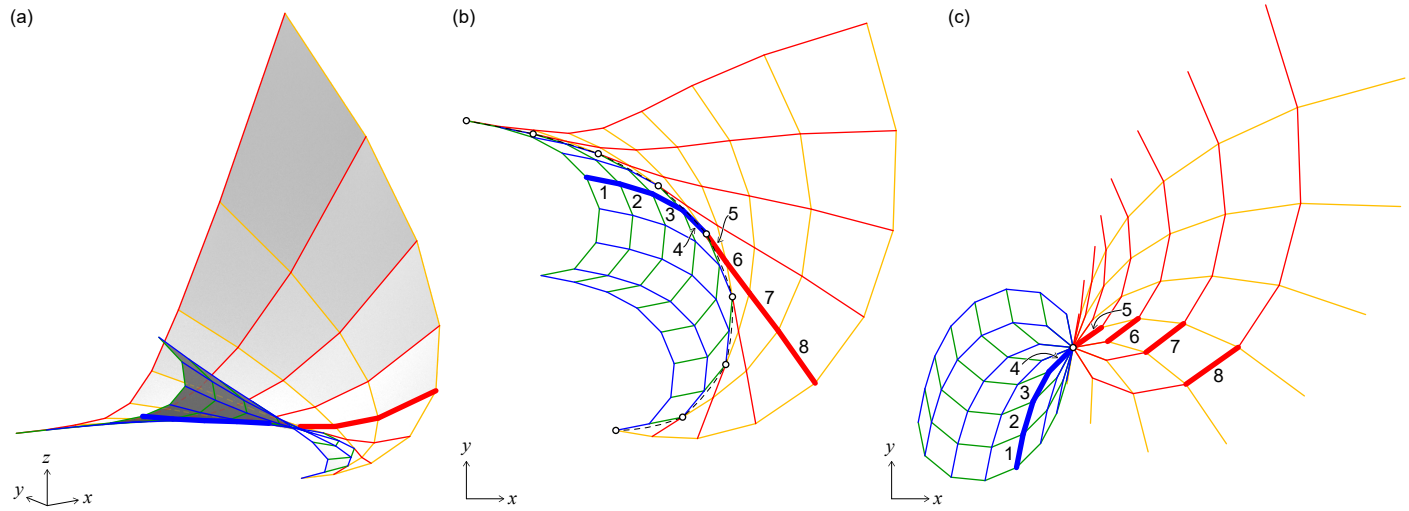

Figure 10: Self-Airy meshes with a discrete singular curve. The negatively curved mesh is shown in blue and green parameter lines, while the positively curved mesh is shown in red and yellow parameter lines. In order to get the 3D mesh (a), one should first work in the top view (b), then use the derivative properties to get the top view of the dual mesh (c). Eight corresponding pairs in (b) and (c) are labeled by numbers.

Furthermore, at $i = j$, the mesh should coincide with the planar curve $c(i)$:

$$R_x(i,i) = c_x(i), \qquad R_y(i,i) = c_y(i). \tag{27d}$$

Due to rank deficiency, equations (27) can not uniquely determine the values of $R_x(i,j)$ and $R_y(i,j)$. One can include the harmonic equation in the diagonal directions:

$$\begin{aligned} R_x(i,j) = \frac{1}{4}\Big[&R_x(i+1,j+1) + R_x(i+1,j-1) \\ &+ R_x(i-1,j+1) + R_x(i-1,j-1)\Big], \end{aligned} \tag{28a}$$

$$\begin{aligned} R_y(i,j) = \frac{1}{4}\Big[&R_y(i+1,j+1) + R_y(i+1,j-1) \\ &+ R_y(i-1,j+1) + R_y(i-1,j-1)\Big]. \end{aligned} \tag{28b}$$

However, equations (27) & (28) will make the problem over-determined. We recommend using weighted least squares and putting much higher weights on equations (27). Therefore, the resulting mesh $(R_x(i,j), R_y(i,j))$ will strongly comply with equations (27) and gently follow the suggestion of equations (28).

Determine the top view of the dual mesh. By remark 8, we can assume that the primal mesh $R(i,j)$ has planar quadrilaterals. Each planar quadrilateral of the primal mesh would be dual to a vertex in the dual mesh. Let $R^\delta(\alpha,\beta)$ denote the vertex in the dual mesh that is corresponding to the quadrilateral formed by vertices $R(\alpha \pm .5, \beta \pm .5)$, where $\alpha, \beta \in \{.5,\ 1.5,\ 2.5, \ldots,\ n-.5\}$.

By discretizing remark 10, we can establish conditions:

$$R^\delta_x(\overset{++}{\alpha},\beta) - R^\delta_x(\alpha,\beta) = \sqrt{\mathrm{i}K}\left[-R_y(\overset{+}{\alpha},\overset{+}{\beta}) + R_y(\overset{+}{\alpha},\overset{-}{\beta})\right], \tag{29a}$$

$$R^\delta_y(\overset{++}{\alpha},\beta) - R^\delta_y(\alpha,\beta) = \sqrt{\mathrm{i}K}\left[\ R_x(\overset{+}{\alpha},\overset{+}{\beta}) - R_x(\overset{+}{\alpha},\overset{-}{\beta})\right], \tag{29b}$$

$$R^\delta_x(\alpha,\overset{++}{\beta}) - R^\delta_x(\alpha,\beta) = \sqrt{\mathrm{i}K}\left[\ R_y(\overset{+}{\alpha},\overset{+}{\beta}) - R_y(\overset{-}{\alpha},\overset{+}{\beta})\right], \tag{29c}$$

$$R^\delta_y(\alpha,\overset{++}{\beta}) - R^\delta_y(\alpha,\beta) = \sqrt{\mathrm{i}K}\left[-R_x(\overset{+}{\alpha},\overset{+}{\beta}) + R_x(\overset{-}{\alpha},\overset{+}{\beta})\right], \tag{29d}$$

where $\overset{++}{\alpha} = \alpha + 1$, $\overset{+}{\alpha} = \alpha + .5$, $\overset{-}{\alpha} = \alpha - .5$, similarly, $\overset{++}{\beta} = \beta + 1$, $\overset{+}{\beta} = \beta + .5$, $\overset{-}{\beta} = \beta - .5$.

The primal mesh $R(i,j)$ at $i = j = t$ coincides with the singular curve $(c_x(t), c_y(t), 0)$, which is contained in the plane $z = 0$. By duality, we can infer the dual mesh $R^\delta(\alpha,\beta)$ at $\alpha = \beta$ should follow the condition

$$R^\delta_x(\alpha,\alpha) = R^\delta_y(\alpha,\alpha) = 0. \tag{29e}$$

The top view of the dual mesh $R^\delta(\alpha,\beta)$ can be uniquely determined by the top view of $R(i,j)$ via equations (29). So far, the heights of both meshes $R_z(i,j)$ and $R^\delta_z(\alpha,\beta)$ remain unknown. The following paragraphs can help us to determine the heights.

Determine the height of the primal and dual meshes. The top view of the primal mesh $R(i,j)$ and the dual mesh $R^\delta(\alpha,\beta)$ are ready, which means the slopes of the meshes are known. As indicated by the duality (§ 2.4), a planar face of $R(i,j)$ is dual to a point of $R^\delta(\alpha,\beta)$:

$$R_z(i,j) + R^\delta_z(\alpha,\beta) = R_x(i,j)\cdot R^\delta_x(\alpha,\beta) + R_y(i,j)\cdot R^\delta_y(\alpha,\beta), \tag{30}$$

where $i = \alpha \pm .5$, $j = \beta \pm .5$, $\alpha, \beta \in \{.5,\ 1.5,\ 2.5, \ldots,\ n-.5\}$.

The duality also works in another way: a point of $R(i,j)$ is dual to a planar face of $R^\delta(\alpha,\beta)$. Equation (30) also works,

just the indices are different: $i, j \in \{1, 2, 3, \ldots, n\}$, $\alpha = i \pm .5$, $\beta = j \pm .5$.

To get the heights of the primal mesh $R_z(i, j)$, we have

$$R_z(\overset{++}{i}, j) - R_z(i, j) = \Big[R_x(\overset{++}{i}, j) - R_x(i, j)\Big] \cdot R_x^\delta(\overset{+}{i}, \overset{+}{j}) + \Big[R_y(\overset{++}{i}, j) - R_y(i, j)\Big] \cdot R_y^\delta(\overset{+}{i}, \overset{+}{j}), \quad (31a)$$

$$R_z(i, \overset{++}{j}) - R_z(i, j) = \Big[R_x(i, \overset{++}{j}) - R_x(i, j)\Big] \cdot R_x^\delta(\overset{+}{i}, \overset{+}{j}) + \Big[R_y(i, \overset{++}{j}) - R_y(i, j)\Big] \cdot R_y^\delta(\overset{+}{i}, \overset{+}{j}), \quad (31b)$$

where $\overset{++}{i} = i + 1$, $\overset{+}{i} = i + .5$, $\overset{-}{j} = j - .5$, $\overset{--}{j} = j - 1$. Since the singular curve is set to be on the plane $z = 0$, at $i = j$, we also have

$$R_z(i, i) = 0. \quad (31c)$$

Equations (31) can sufficiently determine the heights of the primal mesh $R_z(i, j)$.

To get the heights of the dual mesh $R_z^\delta(\alpha, \beta)$, the same procedure we just worked on the primal mesh can also help us to solve the height of the dual mesh:

$$R_z^\delta(\overset{++}{\alpha}, \beta) - R_z^\delta(\alpha, \beta) = \Big[R_x^\delta(\overset{++}{\alpha}, \beta) - R_x^\delta(\alpha, \beta)\Big] \cdot R_x(\overset{+}{\alpha}, \overset{+}{\beta}) + \Big[R_y^\delta(\overset{++}{\alpha}, \beta) - R_y^\delta(\alpha, \beta)\Big] \cdot R_y(\overset{+}{\alpha}, \overset{+}{\beta}), \quad (32a)$$

$$R_z^\delta(\alpha, \overset{++}{\beta}) - R_z^\delta(\alpha, \beta) = \Big[R_x^\delta(\alpha, \overset{++}{\beta}) - R_x^\delta(\alpha, \beta)\Big] \cdot R_x(\overset{+}{\alpha}, \overset{+}{\beta}) + \Big[R_y^\delta(\alpha, \overset{++}{\beta}) - R_y^\delta(\alpha, \beta)\Big] \cdot R_y(\overset{+}{\alpha}, \overset{+}{\beta}), \quad (32b)$$

$$R_z(\alpha, \alpha) = 0, \quad (32c)$$

where $\overset{++}{\alpha} = \alpha + 1$, $\overset{+}{\alpha} = \alpha + .5$, $\overset{-}{\beta} = \beta - .5$, $\overset{--}{\beta} = \beta - 1$.

By equations (27)-(32), one can determine the primal mesh $R(i, j)$ and dual mesh $R^\delta(\alpha, \beta)$. Figure 10 provide an example.

4.3. Area ratio between primal and dual meshes

The area ratio between primal and dual meshes is essentially *isotropic* Gaussian curvature since dual mesh share the same top view as the *isotropic* Gauss image. Thus, we can prove a mesh has a constant *isotropic* Gaussian curvature whenever the area ratio of the primal quadrilaterals and their corresponding dual quadrilaterals is constant.

We first discuss the negatively curved mesh and assume the *isotropic* Gaussian curvature is negative one: ${}^{\mathrm{i}}K = -1$. The vertex stars are all planar since the connecting edges are discrete asymptotic curves (remark 8, theorem 11). Therefore, one can easily define the dual vertex of each vertex star. The area of the primal quadrilateral constructed by the adjacent points of a vertex is composed of four triangles. These triangles correspond to four dual triangles. Each dual edge is orthogonal to the corresponding primal edge. Also, from § 2.4, we know that the dual asymptotic edges have the same lengths as the primal edges when ${}^{\mathrm{i}}K = -1$. Thus, a primal triangle and the corresponding dual triangle have the same area ($ab \sin\theta = ab \sin(\pi - \theta)$, fig. 11). The dual triangles form the dual quadrilateral. These primal quadrilaterals and the dual quadrilaterals respectively completely cover the primal and the dual mesh twice. Thus, we know the area ratio of primal and dual mesh is indeed constant for individual vertex stars and for whole meshes.

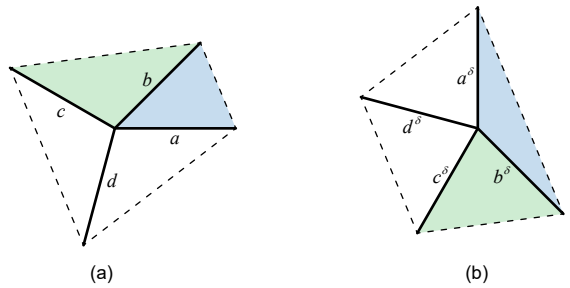

Figure 11: A pair of dual vertex stars for negatively curved meshes (${}^{\mathrm{i}}K = -1$). The edges $a, b, \ldots$ respectively correspond to edges $a^\delta, b^\delta, \ldots$. The triangles of the same color have the same area.

Now we shift our attention to a positively curved mesh and assume the *isotropic* Gaussian curvature is one: ${}^{\mathrm{i}}K = 1$. The mesh is conjugate, and therefore the quadrilaterals are planar. Each quadrilateral corresponds to a vertex in the dual mesh, and vice versa. The area of the primal quadrilateral constructed by the adjacent points of a regular vertex is twice the area of the corresponding dual quadrilateral (fig. 12). Such primal quadrilaterals completely cover the primal mesh twice. As a result, the sum of the areas is twice the area of the primal mesh. The corresponding dual quadrilaterals also completely cover the dual mesh. Therefore, we can be sure the area ratio of primal and dual meshes is indeed constant for each vertex star and its corresponding rectangle, as well as for whole meshes.

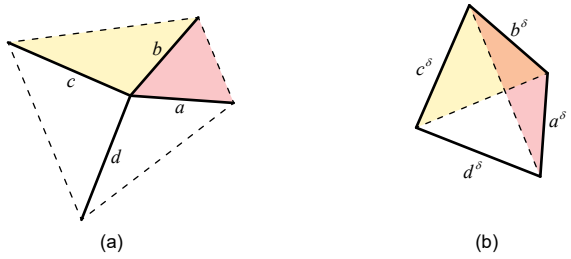

Figure 12: A dual vertex star and its corresponding quadrilateral for positively curved meshes (${}^{\mathrm{i}}K = 1$). The edges $a, b, \ldots$ respectively correspond to edges $a^\delta, b^\delta, \ldots$. The triangles of the same color have the same area.

5. Singularities and stitching regular patches

Section 4 has shown how to generate *regular quadrilateral* meshes from a single discrete curve. A *regular quadrilateral* mesh has each vertex connected by 4 edges and each polygon bounded by 4 edges. Although one can arbitrarily design the discrete curve (thus the shape of the unenforced edge), a single unreinforced edge is too limiting for architectural design.

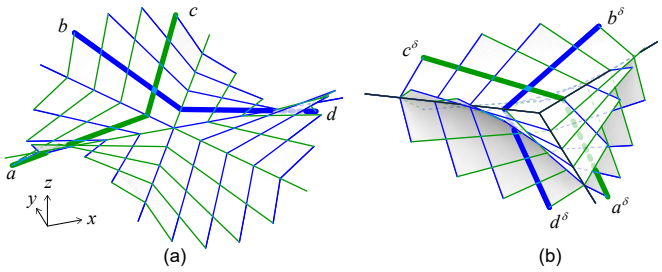

Figure 13: A pair of dual negatively curved self-Airy meshes. The primal mesh (a) has a valence-6 singular point. The dual mesh is self-intersecting (b). The primal singular point corresponds to the "pinch point" in the dual mesh. Two highlighted parameter lines $\overline{ac}$ and $\overline{bd}$ correspond to $\overline{a^\delta c^\delta}$ and $\overline{b^\delta d^\delta}$

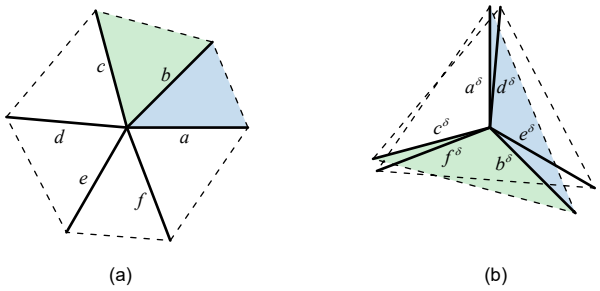

Figure 14: A pair of dual valence-6 vertex stars for negatively curved meshes (${}^{\mathrm{i}}K = -1$). The edges $a, b, \ldots$ respectively correspond to edges $a^\delta, b^\delta, \ldots$. The triangles of the same color have the same area.

This section is going to explore wider solutions: *semiregular quadrilateral* meshes that have a few singular points (vertices connected by 5 or more edges) or singular polygons (polygons bounded by 5 or more edges). With the singularity, designers of self-Airy shells can stitch regular patches to create much more interesting forms and incorporate more than one unreinforced edge to a design.

5.1. Negatively curved mesh with a singular point

Large negatively curved constant Gaussian curvature surfaces (e.g., hyperbolic surfaces) tend to have singular points and curvature discontinuity [34]. Shearman and Venkataramani [34] have pointed out that, at the singular or "branch" point, there are $n \geq 3$ asymptotic directions. In contrast, a regular point has only 2 asymptotic directions, which divide the neighborhood region into 4 "sectors". Two of them are above the tangent plane, while the other two are below. At a singular point of 3 (or n) asymptotic directions, there are 6 (or $2n$) sectors, of which 3 (or n) are above the tangent plane, whereas the other 3 (or n) are below.

The asymptotic curves emanating from the "branch" points divide the surfaces into patches. Within a patch, the surface can enjoy C^∞ smoothness, but, at the transition curves between patches, the maximum continuity is C^1. Shearman and Venkataramani's [34] observation in Euclidean geometry also extends to *isotropic* geometry as well as the discrete setting. Therefore, for the negatively curved constant ${}^{\mathrm{i}}K$ meshes, asymptotic lines crossing through the patch boundaries will have intense geodesic curvature (fig. 13).

The singular points correspond to "pinch points" at their dual surfaces. As a result, surfaces with such a singularity have self-intersecting dual surfaces. The discretized mesh has the same properties (fig. 13).

These singularities may cripple the constant area ratio of primal and dual meshes. For instance, an *isotropic* translation net consisting of mostly quadrilaterals and a singular hexagon would find the area ratio of the primal hexagon and the self-intersecting dual hexagon different from the ratio of the pairs of regular quadrilaterals. When the self-Airy surface is divided into a finer mesh, the area of the singular hexagon is less prominent, and thus the mesh is closer to the ideal self-Airy surface. However, a coarse *isotropic* translation net consisting of only quadrilaterals (even having singular valence-6 vertices) can have a dual mesh of constant area ratio and thus constant *isotropic* Gaussian curvature (fig. 14).

One may like to seek whether there is a self-Airy mesh consisting of point supports (conical singularities) and unreinforced edges (planar singular curves). There exist negatively curved constant ${}^{\mathrm{i}}K$ meshes with two point supports and two segments of unreinforced boundary. However, there is no obvious solution of a negatively curved constant ${}^{\mathrm{i}}K$ mesh with $n \geq 3$ point supports and $n \geq 3$ segments of unreinforced boundary without degenerate quadrilaterals. The condition of being a "translation net" in the top view is quite restrictive. A close solution as well as a degenerate solution of a 3-support mesh are included in § 6.

5.2. Positively curved mesh with a singular point

As remark 7 suggests, Strubecker's construction for a positively curved constant ${}^{\mathrm{i}}K$ surface has a harmonic net in the top view. The condition of a harmonic net is less restrictive than that of a translation net. As a result, in the discrete setting, one can easily find a harmonic mesh with 3 or more singular point supports and singular boundaries. The discretized harmonic conditions (27) can be generalized as the top view of each vertex (R_x, R_y) sitting at the barycenter of the adjacent n vertices (R_{xi}, R_{yi}), $1 \geq i \geq n$:

$$(R_x, R_y) = \frac{1}{n} \sum_{i=1}^{n} (R_{xi}, R_{yi}). \tag{33}$$

The $n = 2$ when the point (R_x, R_y) is at the singular curve; the $n = 4$ when the point is a regular interior point; the $n \geq 5$ when the point is a singular interior point.

Equation (33) is equivalent to the 2D equilibrium of nodes in a network of springs, in which the relaxed lengths are zero and the spring constants are identical (see [14] and [56]). The equilibrium of such a network can be represented by an Airy stress function, which is automatically a polyhedral surface. Figures 15a & b respectively provide a network of springs and its polyhedral Airy stress function R. The dual mesh R^δ also automatically satisfies equations (29). A self-Airy mesh of *isotropic* Gaussian curvature ${}^{\mathrm{i}}K$ is associated with a spring network of spring constant $k = \sqrt{{}^{\mathrm{i}}K}$.

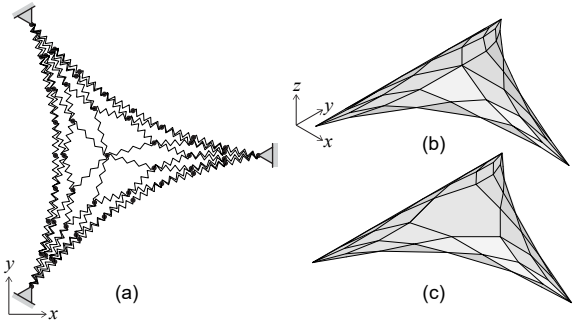

Figure 15: A simple example of a spring network (a) and its polyhedral Airy stress function (b) as well as the dual mesh of the Airy stress function (c).

Such a positively curved self-Airy mesh is uniquely defined by its topology and its support points, since the positions of all the vertices are determined by the harmonic condition (33). Topology refers to the mesh's connectivity properties—how its vertices, edges, and faces are arranged and connected. Figure 16 shows a series of self-Airy meshes. All these meshes have 1 valence-6 singular point at the center, 3 point supports, and 3 segments of unreinforced boundary. The difference is in the topology distances from the center to the point supports or the unreinforced boundary. The topology structure affects the shape of unreinforced boundaries as well as the value of the *isotropic* Gaussian curvature.

However, around singular vertex stars, the area ratios between the primal and dual meshes are not constant. As § 4.3 shows, for a regular mesh of ${}^{\mathrm{i}}K = 1$, the area of the primal quadrilateral constructed by the adjacent points of a regular vertex is twice the area of the dual corresponding quadrilateral. For a singular vertex of valence-n, the area of the n-polygon constructed by the adjacent points is twice the area of the corresponding n-polygon minus the $n/2$ star polygon. Figure 17 shows an example of valence-6 vertex star and its dual hexagon, where the area deficit is the hexagram. When the mesh becomes denser, the deficit becomes smaller (fig. 18).

It is also possible to locate a pentagon next to a singular vertex of valence-5, which respectively dual to a valence-5 vertex start and a pentagon. This arrangement produces two $5/2$ star polygons. One of them is deficit while the other is surplus. When the shapes of the pentagons are the same, the $5/2$ star polygons have the same area and thus the deficit is neutralized by the surplus (fig. 18).

6. Application

This section presents a few examples that utilize the proposed method of constructing constant *isotropic* Gaussian curvature meshes to conceptually design self-Airy shells for roof-like structures.

6.1. Negatively curved self-Airy shells with two supports

Figure 19 shows a series of self-Airy shells that result from Strubecker's construction taking curves of double rotational symmetry as input. Since the curves are symmetric with respect

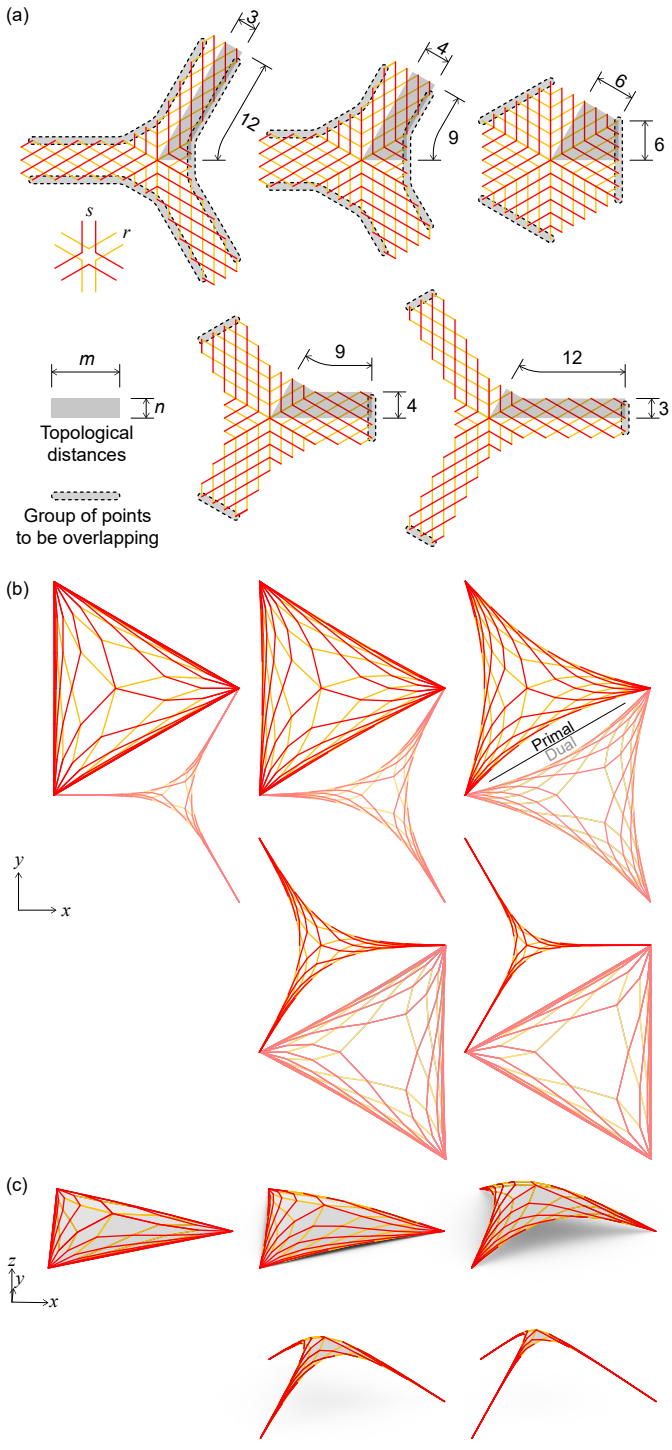

Figure 16: The topological input affects the shape of the unreinforced boundaries. (a) Five topological inputs of different topological distances from the center to the unreinforced boundary and the support. (b) The results of solving equations (27-29). (c) The results of solving equations (31). The longer the distance from the center to the support, the larger the Gaussian curvature.

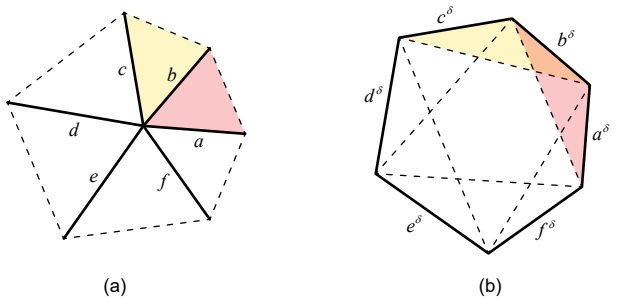

Figure 17: A dual vertex star and its corresponding hexagon for positively curved meshes (${}^{\mathrm{i}}K = 1$). The edges $a, b, \ldots$ respectively correspond to edges $a^\delta, b^\delta, \ldots$. The triangles of the same color have the same area. The 6/2 star polygon in (b) will not completed covered by the 6 triangles.

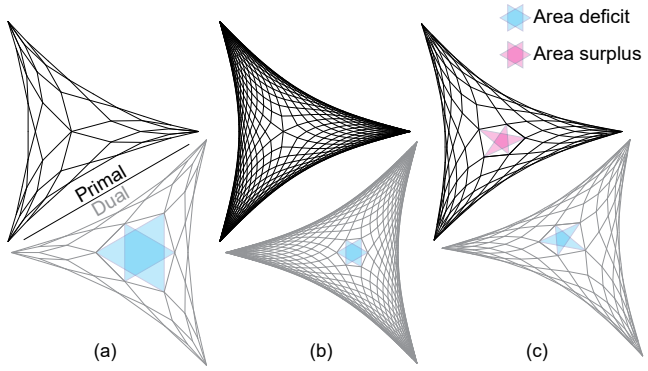

Figure 18: Harmonic meshes and their dual. When the dual mesh is considered as the top view of the Gauss image, we can observe a singular vertex star would have an area deficit (or a curvature surplus), which has higher local Gaussian curvature. The primal mesh in (b) has a denser network and therefore has a smaller area deficit than the case in (a). A singular polygon in the primal mesh creates an area surplus (or a curvature deficit).

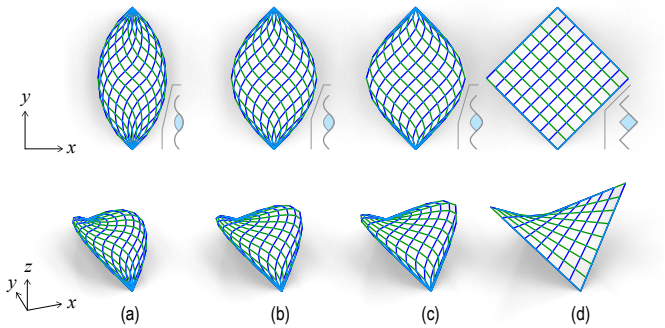

Figure 19: Negatively curved self-Airy shells which originate from double rotational symmetry curves. The top row shows top views as well as the associated curves in a lighter shade at the side. The bottom row shows axonometric views.

to two points, the resulting surface will have a conical singularity at each of these points. Let $c(t)$ denote such a planar curve that passes through the symmetrical centers c_i ($i \in \{1, 2\}$)) when $t = t_i$. Provided the curve is rotationally symmetric with respect to t_i, we can infer $c(t_i + \Delta t) + c(t_i - \Delta t) = 2c_i$. The top view of Strubecker's construction (10) yields the surface $S(u, v)$, which has singular points at points c_i when the parameters adhere to $u + v = 2t_i$.

Furthermore, the resulting surface has two planar singular curves. The obvious one traces $u - v = 0$. The less obvious one follows $u - v = 2(t_1 - t_2)$. On $u - v = 2(t_1 - t_2)$, one has the straight line segment $C(u, v)$ with end points $c(u)$ & $c(v)$ and its midpoint $m(u, v) = [c(u) + c(v)]/2$ that are moving parallelly. Since the straight line segment has a constant length of $\|c_1 - c_2\|$, the $u - v = 2(t_1 - t_2)$ traces a planar curve. Since Strubecker's construction gives a constant *isotropic* Gaussian curvature surface for any pair of (u, v), this planar curve must be singular.

One can tilt the resulting surface by an affine map to make both the unreinforced boundaries incline and only leave the singular points touching the ground. Architects may want to build such surfaces. Although there are only two supports, which are insufficient to stably fix a structure, engineers can add minor secondary supports to stabilize the structure. Therefore, after some adjustment, these surfaces are still practical to be physically built.

When the curve approaches a zigzag, one can notice that part of the asymptotic net degenerates into straight lines at the boundaries. These boundaries are still free and do not need extra support to reach equilibrium. However, reinforcements are needed to take care of the concentrated axial load. The result of a zigzag is a hyperbolic paraboloid which was a popular shape for shells in the 1950s to the 60s. The Spanish-Mexican architect and engineer Félix Candela (1910-1977) extensively used this shape in his ingenious designs [57].

6.2. *Negatively curved roofs with three supports*

Designers can introduce singular points to combine regular patches into an interesting whole. Here, we introduce a singular point of valence-6 and design a mesh of three supports. If one insists that, except at the conical singular points, there should be no degenerate quadrilaterals, one may only find self-Airy meshes similar to the one shown in figure 20(a), which has short linear supports between conical point supports and the unreinforced boundaries. If one allows degenerate quadrilaterals, one can assemble a mesh similar to the case shown in figure 20(c), which has three conical point supports directly adjacent to unsupported boundaries.

Dual meshes of self-Airy meshes are also self-Airy meshes, as discussed in § 2.4. Figures 20(b) & (d) respectively show the dual meshes of the primal meshes shown in (a) & (c). These dual meshes have a pinch point and therefore are self-intersecting. Although they are not suitable for a practical roof-like structure, they might serve as inspiration for art installations. A minor remark is that, as the shell in (a) has short segments of linear supports, its dual shell in (b) would require extra struts for supporting.

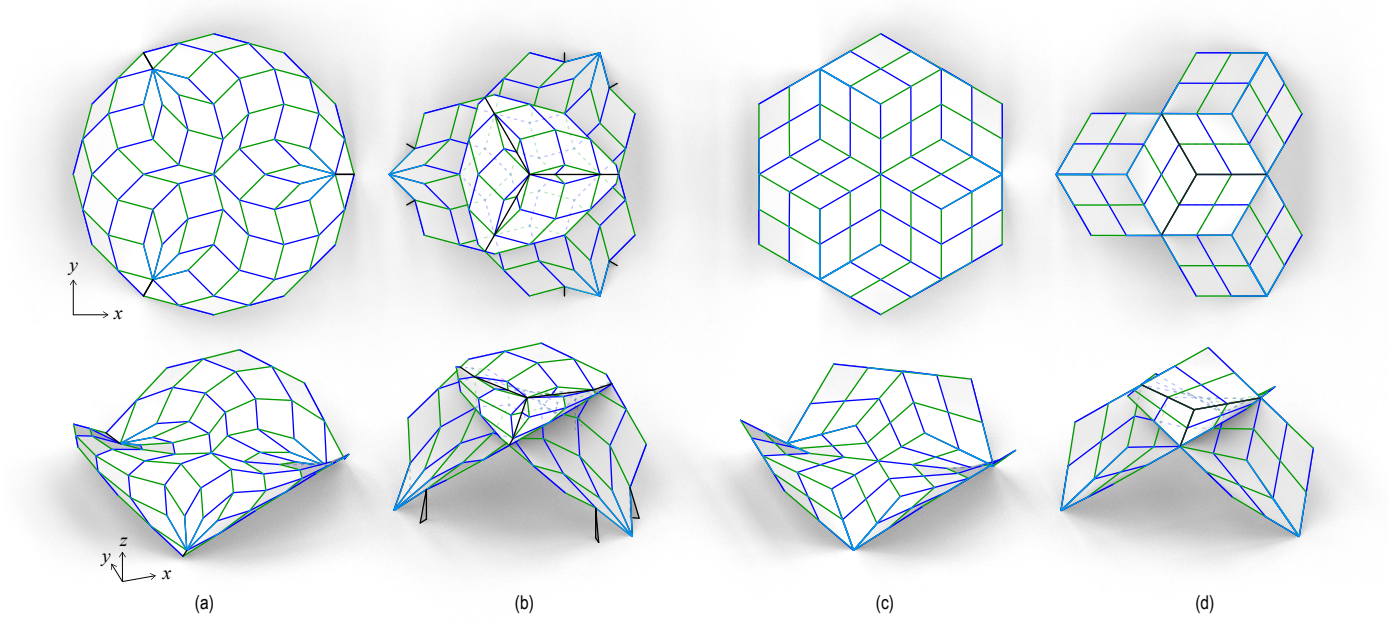

Figure 20: Two pairs of dual meshes, which are negatively curved self-Airy meshes with three supports. Mesh (a) is dual to mesh (b), while mesh (c) is dual to mesh (d). Since each support of mesh (a) consists of a conical point and two segments, its dual support features an unreinforced boundary and two shear walls. In contrast, since each support of mesh (c) consists only of a conical point, its dual support consists solely of an unreinforced boundary.

6.3. Four point supports for positively curved roofs

Singular points can also combine positively curved patches. To generate a four-point-support shell, one can use one of the various singular structures, for example:

1. one valence-8 singular point (fig. 21a),
2. two valence-6 singular points (fig. 21c),
3. two valence-5 singular points with two 5-sided singular polygons (fig. 21e), and
4. the duals of the above cases (respectively, fig. 21b, d, & e).

The boundaries of these positively curved meshes can contain only point supports and unreinforced segments, unlike the negatively curved case in figure 20a which must have short segments of linear supports. Each of the primal meshes (fig. 21a, c, & d) has 4 point supports and 4 segments of unreinforced boundaries. Since a point support is dual to an unreinforced boundary and vice versa, each of the dual meshes (fig. 21b, d, & e) contain 4 segments of unreinforced boundaries and 4 point supports.

Some of the four point supports may need to be elevated since they may not be coplanar. As discussed in § 5.2, after designers choose the mesh topology and the top view of the supporting points, the top view of the unreinforced boundaries will be uniquely determined by the harmonic condition (33). The height is also subsequently determined by equations (29-31). The only left freedom is the affine shearing in the z-direction $(x,y,z) \mapsto (x, y, z+ax+by+d)$, which has 3 degrees of freedom. Since the number of point supports exceeds the affine shearing map's degrees of freedom, it is generally not possible for leveling the point supports of an arbitrary self-Airy mesh. However, if the topology and the support points are arranged in a symmetric manner, the four points can still be leveled as in the cases in figure. 21a, b, & c, while two point supports of the meshes in figure. 21d, e, & f are elevated.

6.4. Roof of mixing positively and negatively curved meshes

We can combine positively and negatively curved meshes along the unreinforced boundary to generate more interesting results. For a positively curved self-Airy mesh, the top view of the unreinforced boundary is dictated by the harmonic condition (33). Conversely, for a negatively curved self-Airy mesh of two supports, the boundary is free to accept an arbitrary curve. Then, it becomes obvious that we should first determine the positively curved part. Based on the "form-found" unreinforced boundary, we then shape the negatively curved self-Airy mesh accordingly.

We can stitch the positively and negatively curved meshes tightly or leave a gap between them. The roof shown in figure 22 features a positively curved mesh at the center and four segments of unreinforced boundaries. Two of these are tightly connected to two negatively curved meshes, while the other two are connected to another pair of negatively curved meshes through skylights. Owing to the planarity of the unreinforced boundaries, we can make one of the skylights planar, while the other one is prismatic.

7. Conclusion

Contributions. This paper has reviewed the features of self-Airy shells and identified its unreinforced boundaries as planar

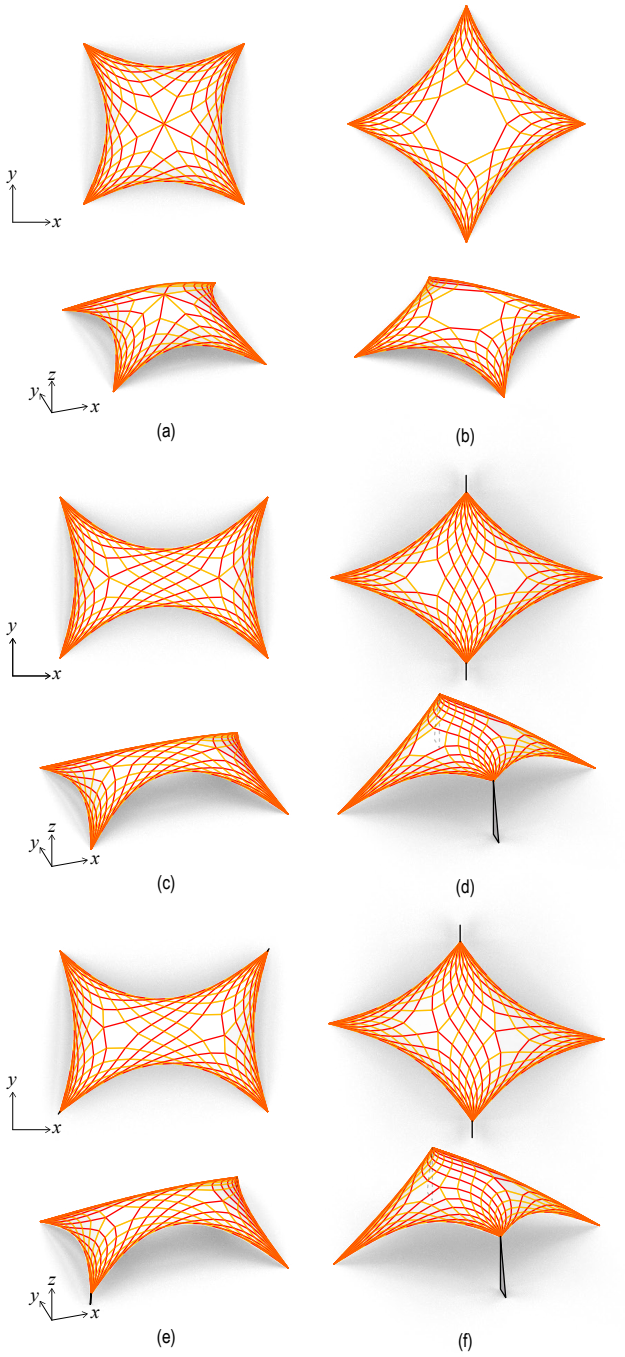

Figure 21: Three pairs of dual meshes, which are positively curved self-Airy meshes with four supports. (a & b) A pair of dual meshes. The valence-8 singular point in (a) is dual to the 8-sided singular polygon in (b). (c & d) and (e & f) are the other two pairs. A valence-n singular point dual to a n-sided polygon.

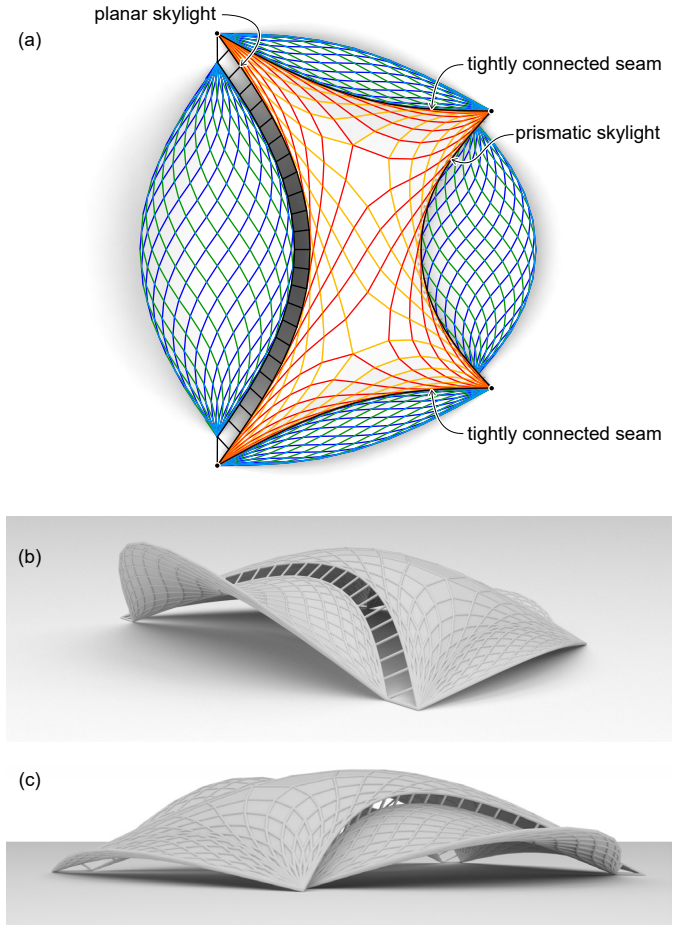

Figure 22: A roof mixing positively and negatively curved meshes. (a) Top view. (b & c) Perspective views respectively looking towards the planar skylight and the prismatic one. (d) An internal view.

singular curves. We have also reviewed the important contribution of Strubecker's early works on smooth constant *isotropic* Gaussian curvature surfaces and his construction of such surfaces from arbitrary planar singular curves. We have proposed a systematic approach to convert Strubecker's construction into the discrete counterpart for both positively and negatively curved constant *isotropic* Gaussian curvature meshes. The former positively curved cases, which require the complex extension, are also converted into real parameters which allow users to deal with much ease.

Beyond the construction of regular quadrilateral meshes, we also proposed the method for building up semi-regular quadrilateral meshes, which contain singular points. For negatively curved meshes, the asymptotic net will have kink angles crossing the bounders between regular patches. For positively curved meshes, the parametric net remains smooth. Yet, a singular vertex star (dual to a singular polygon) will have an area deficit, which can be reduced by a finer subdivision.

A few designs of roof-like structures are also presented. Designers can generate various self-Airy shells with unreinforced boundaries. Mixing positively and negatively curved self-Airy shells in one design is also demonstrated.

Future Work. This paper assumes the load is vertical and uniformly distributed per horizontal area, therefore the resulting surfaces are constant *isotropic* Gaussian curvature surfaces. These surfaces can be the basis for future research in at least three directions:

1. Offset the meshes into *isotropic* linear Weingarten surfaces and explore the wider range of design domains.
   Offsetting a constant *isotropic* Gaussian curvature surface will yield an *isotropic* linear Weingarten surface, which admits a stress distribution of which the principal orientation aligns with the one of curvature.
2. Refine the resulting meshes into constant Gaussian curvature surfaces in terms of the Euclidean metric.
   Such a surface would be the Euclidean counterpart of the self-Airy surface that withstands a uniformly distributed normal stress. One of the simplest examples would be a sphere under uniform pressure.
3. Amend the meshes to have *isotropic* Gaussian curvature proportional to the tilting area.
   As discussed in § 2.2, the more realistic load intensity should be proportional to the tilting area. Since the vertical load of a self-Airy surface is proportional to its *isotropic* Gaussian curvature, amending the curvature distribution is to adopting the realistic load distribution.

The first direction would be relatively straightforward compared to the other two. Both the second and the third directions make the problem non-linear. The later two directions require the linear proportionality between the area of each facet and the area of its Gauss image, to be more precise, Euclidean Gauss image for the second direction while *isotropic* Gauss image for the third direction. One can reformulate the problem as an optimization problem to minimize the deviation of the ratio between the areas. Nonetheless, the results from this paper would serve as convenient inputs to initialize the non-linear optimization process.

CRediT authorship contribution statement

Y.-C. Chiang: Conceptualization, Methodology, Software, Visualization, Writing - Original draft preparation, Writing - Reviewing and Editing. **H. Wang**: Software, Visualization. **X. Li**: Visualization, Validation. **H. Pottmann**: Investigation, Methodology, Writing - Original draft preparation, Writing - Reviewing and Editing.

Funding

This work was partially supported by the National Science and Technology Council (Taiwan) [grant numbers NSTC 113-2222-E-005-001-MY2]

Declaration of competing interest

The authors declare that they have no known competing financial interests or personal relationships that could have appeared to influence the work reported in this paper.

References

[1] P. Csonka, Theory and practice of membrane shells, VDI Verlag, Düsseldorf, 1987.
[2] A. Fraddosio, N. Lepore, M. D. Piccioni, Thrust surface method: An innovative approach for the three-dimensional lower bound limit analysis of masonry vaults, Engineering Structures 202 (2020) 109846. doi:10.1016/j.engstruct.2019.109846.
[3] Y.-C. Chiang, A. Borgart, A form-finding method for membrane shells with radial basis functions, Engineering Structures 251 (2022) 113514. doi:10.1016/j.engstruct.2021.113514.
[4] C. Millar, T. Mitchell, A. Mazurek, A. Chhabra, A. Beghini, J. N. Clelland, A. McRobie, W. F. Baker, On designing plane-faced funicular grid-shells, International Journal of Space Structures (2022). doi:10.1177/09560599221126656.
[5] J. Chilton, The Engineer's Contribution to Contemporary Architecture: Heinz Isler, Thomas Telford, 2000.
[6] D. Pellis, H. Pottmann, Aligning principal stress and curvature directions, in: Advances in Architectural Geometry 2018, Gothenburg, 2018, pp. 34–53. URL: https://research.chalmers.se/en/publication/504188.
[7] D. Liu, D. Pellis, Y.-C. Chiang, F. Rist, J. Wallner, H. Pottmann, Deployable strip structures, ACM Transactions on Graphics 42 (2023).
[8] C. Rogers, W. Schief, On the equilibrium of shell membranes under normal loading. hidden integrability, Proceedings of the Royal Society of London. Series A: Mathematical, Physical and Engineering Sciences 459 (2003) 2449–2462.
[9] X. Tellier, C. Douthe, L. Hauswirth, O. Baverel, Form-finding with isotropic linear Weingarten surfaces, in: Advances in Architectural Geometry 2020, Champs-sur-Marne, 2021.
[10] K. Strubecker, Differentialgeometrie des isotropen Raumes V. Zur Theorie der Eilinien, Mathematische Zeitschrift 51 (1949) 1432–1823. doi:10.1007/BF01181547.
[11] F. Aish, S. Joyce, S. Malek, C. J. Williams, The use of a particle method for the modelling of isotropic membrane stress for the form finding of shell structures, Computer-Aided Design 61 (2015) 24–31.
[12] H. Pottmann, M. Eigensatz, A. Vaxman, J. Wallner, Architectural geometry, Computers & Graphics 47 (2015) 145–164. doi:10.1016/j.cag.2014.11.002.
[13] M. R. Barnes, Form-finding and analysis of prestressed nets and membranes, Computers & Structures 30 (1988) 685–695.
[14] H.-J. Schek, The force density method for form finding and computation of general networks, Computer Methods in Applied Mechanics and Engineering 3 (1974) 115–134. doi:10.1016/0045-7825(74)90045-0.
[15] P. Block, J. Ochsendorf, Thrust network analysis: A new methodology for three-dimensional equilibrium, Journal of the International Association for Shell and Spatial Structures 48 (2007) 167–173.
[16] E. Vouga, M. Höbinger, J. Wallner, H. Pottmann, Design of self-supporting surfaces, ACM Transactions on Graphics 31 (2012). doi:10.1145/2185520.2185583.
[17] M. Miki, E. Adiels, W. Baker, T. Mitchell, A. Sehlström, C. J. Williams, Form-finding of shells containing both tension and compression using the airy stress function, International Journal of Space Structures 37 (2022) 261–282.
[18] M. Konstantatou, W. Baker, T. Nugent, A. McRobie, Grid-shell design and analysis via reciprocal discrete airy stress functions, International Journal of Space Structures 37 (2022) 150–164.
[19] Y. Shen, J.-P. Jasienski, P. O. Ohlbrock, P. D'acunto, Computational form-finding of single-layer spatial structures: Constructing force diagrams with vector-based graphic statics and guiding trails, Automation in Construction 166 (2024) 105519.
[20] C. Chianese, L. Rosati, F. Marmo, Isogeometric form finding of membrane shells by optimised airy stress function, Computer Methods in Applied Mechanics and Engineering 426 (2024) 116946.
[21] F. Gil-Ureta, N. Pietroni, D. Zorin, Reinforcement of general shell structures, ACM Transactions on Graphics 39 (2020) 1–19.
[22] F. Laccone, N. Pietroni, P. Cignoni, L. Malomo, Bending-reinforced grid shells for free-form architectural surfaces, Computer-Aided Design 168 (2024) 103670.
[23] M. Akbarzadeh, T. Van Mele, P. Block, On the equilibrium of funicular polyhedral frames and convex polyhedral force diagrams, CAD Computer Aided Design 63 (2015) 118–128. doi:10.1016/j.cad.2015.01.006.

[24] A. McRobie, M. Konstantatou, G. Athanasopoulos, G. Torpiano, C. Millar, W. Baker, Simple rankine gridshells, in: Proceedings of IASS Annual Symposia, volume 2020, International Association for Shell and Spatial Structures (IASS), 2020, pp. 1–13.
[25] Y.-C. Chiang, Maxwell-Rankine stress functions of membrane shells and their relation to that of planar funicular gridshells, International Journal of Solids and Structures (2022) 111768.
[26] Y. Liu, H. Pottmann, J. Wallner, Y.-L. Yang, W. Wang, Geometric modeling with conical meshes and developable surfaces, in: ACM SIGGRAPH 2006 Papers, Association for Computing Machinery, New York, 2006, p. 681–689. URL: https://doi.org/10.1145/1179352.1141941. doi:10.1145/1179352.1141941.
[27] R. Mesnil, C. Douthe, C. Richter, O. Baverel, Fabrication-aware shape parametrisation for the structural optimisation of shell structures, Engineering Structures 176 (2018) 569–584. doi:10.1016/j.engstruct.2018.09.026.
[28] Z. Tošić, M. F. Eichenauer, E. Ivaniuk, D. Lordick, S. Krasić, V. Mechtcherine, Design and optimization of free-form surfaces for modular concrete 3d printing, Automation in Construction 141 (2022) 104432.
[29] C. Wang, C. Jiang, H. Wang, X. Tellier, H. Pottmann, Architectural structures from quad meshes with planar parameter lines, Computer-Aided Design 156 (2023) 103463.
[30] X. Tellier, L. Hauswirth, C. Douthe, O. Baverel, Discrete cmc surfaces for doubly-curved building envelopes, in: Advances in Architectural Geometry 2018, 2018.
[31] K. Hayashi, Y. Jikumaru, M. Ohsaki, T. Kagaya, Y. Yokosuka, Discrete gaussian curvature flow for piecewise constant gaussian curvature surface, Computer-Aided Design 134 (2021) 102992.
[32] J. Ochsendorf, P. Block, Exploring shell forms, in: S. Adriaenssens, P. Block, D. Veenendaal, C. Williams (Eds.), Shell Structures for Architecture, Routledge, Abingdon, 2014, pp. 7–12.
[33] Y.-C. Chiang, Design and fabrication of shell structures: Aided by radial basis functions and reconfigurable mechanisms, Ph.D. thesis, Delft University of Technology, 2022. doi:10.7480/abe.2022.03.
[34] T. L. Shearman, S. C. Venkataramani, Distributed branch points and the shape of elastic surfaces with constant negative curvature, J. Nonlinear Science 31 (2021).
[35] G. B. Airy, On the Strains in the Interior of Beams, Philosophical Transactions of the Royal Society of London 153 (1863) 49–79.
[36] J. Heyman, Equilibrium of shell structures, Oxford University Press, Oxford, 1977.
[37] A. Pucher, Über den spannungszustand in gekrümmten flächen, Beton und Eisen 33 (1934) 298–304.
[38] S. P. Timoshenko, S. Woinowsky-Krieger, Theory of plates and shells, McGraw-Hill, 1959.
[39] M. Miki, T. Igarashi, P. Block, Parametric self-supporting surfaces via direct computation of Airy stress functions, ACM Transactions on Graphics 34 (2015). doi:10.1145/2766888.
[40] H. Pottmann, Y. Liu, Discrete surfaces in isotropic geometry, in: IMA International Conference on Mathematics of Surfaces, Springer, Berlin, 2007, pp. 341–363. doi:10.1007/978-3-540-73843-5_21.
[41] H. Sachs, Isotrope Geometrie des Raumes, Vieweg, 1990.
[42] C. Williams, A. McRobie, Graphic statics using discontinuous Airy stress functions, International Journal of Space Structures 31 (2016) 121–134. doi:10.1177/0266351116660794.
[43] K. Strubecker, Differentialgeometrie des isotropen Raumes I: Theorie der Raumkurven, Sitzungsber. Akad. Wiss. Wien 150 (1941) 1–53.
[44] K. Strubecker, Differentialgeometrie des isotropen Raumes II: Die Flächen konstanter Relativkrümmung $K = rt - s^2$, Math. Zeitschrift 47 (1942) 743–777.
[45] K. Strubecker, Differentialgeometrie des isotropen Raumes III: Flächentheorie, Math. Zeitschrift 48 (1942) 369–427.
[46] K. Strubecker, Differentialgeometrie des isotropen Raumes IV: Theorie der flächentreuen Abbildungen der Ebene, Math. Zeitschrift 50 (1944) 1–92.
[47] K. Strubecker, Airysche Spannungsfunktion und isotrope Differentialgeometrie, Mathematische Zeitschrift 78 (1962) 434–459. doi:10.1007/BF01195167.
[48] C. Maxwell, On reciprocal figures and diagrams of forces, The London, Edinburgh, and Dublin Philosophical Magazine and Journal of Science 27 (1864) 250–261. doi:10.1080/14786446408643663.
[49] C. Maxwell, On Reciprocal Diagrams in Space and their relation to Airy's Function of Stress, Proceedings of the London Mathematical Society 1 (1868) 58–63.
[50] C. Maxwell, On reciprocal figures, frames, and diagrams of forces, Earth and Environmental Science Transactions of the Royal Society of Edinburgh 26 (1870) 1–40.
[51] K. Strubecker, Differentialgeometrie III: Theorie der Flächenkrümmung, de Gruyter, 1969.
[52] H. Crapo, W. Whiteley, Spaces of stresses, projections and parallel drawings for spherical polyhedra, Contributions to Algebra and Geometry 35 (1994) 259–281.
[53] M. Konstantatou, P. D'Acunto, A. McRobie, Polarities in structural analysis and design: n-dimensional graphic statics and structural transformations, International Journal of Solids and Structures 152 (2018) 272–293.
[54] M. E. Aydin, Classifications of translation surfaces in isotropic geometry with constant curvature, 2016. ArXiv: 1612.09061.
[55] A. I. Bobenko, Y. B. Suris, Discrete differential geometry. Integrable structure, volume 98 of *Graduate Studies in Mathematics*, American Mathematical Society, Providence, RI, 2008.
[56] D. Veenendaal, P. Block, An overview and comparison of structural form finding methods for general networks, International Journal of Solids and Structures 49 (2012) 3741–3753. doi:10.1016/j.ijsolstr.2012.08.008.
[57] S. Wang, M. Garlock, B. Glisic, Geometric and area parameterization of n-edged hyperbolic paraboloidal umbrellas, Engineering Structures 250 (2022) 113499. doi:10.1016/j.engstruct.2021.113499.

Appendix A. Derivatives of Strubecker's construction

From Strubecker's construction (10), the parametric surface $S(u, v)$ has the first and second derivatives:

$$S_{,u} = \left(\frac{\dot{c}_x(u)}{2}, \frac{\dot{c}_y(u)}{2}, \frac{\sqrt{-\mathrm{i}K}}{4}\Big\{\dot{c}_x(u)[c_y(u) - c_y(v)] - \dot{c}_y(u)[c_x(u) - c_x(v)]\Big\}\right), \tag{A.1}$$

$$S_{,v} = \left(\frac{\dot{c}_x(v)}{2}, \frac{\dot{c}_y(v)}{2}, \frac{\sqrt{-\mathrm{i}K}}{4}\Big\{\dot{c}_x(v)[c_y(u) - c_y(v)] - \dot{c}_y(v)[c_x(u) - c_x(v)]\Big\}\right), \tag{A.2}$$

$$S_{,uu} = \left(\frac{\ddot{c}_x(u)}{2}, \frac{\ddot{c}_y(u)}{2}, \frac{\sqrt{-\mathrm{i}K}}{4}\Big\{\ddot{c}_x(u)[c_y(u) - c_y(v)] - \ddot{c}_y(u)[c_x(u) - c_x(v)]\Big\}\right), \tag{A.3}$$

$$S_{,uv} = \left(0,\ 0,\ \frac{\sqrt{-\mathrm{i}K}}{4}\Big\{ - \dot{c}_x(u)\dot{c}_y(v) + \dot{c}_y(u)\dot{c}_x(v)\Big\}\right), \tag{A.4}$$

$$S_{,vv} = \left(\frac{\ddot{c}_x(v)}{2}, \frac{\ddot{c}_y(v)}{2}, \frac{\sqrt{-\mathrm{i}K}}{4}\Big\{\ddot{c}_x(v)[c_y(u) - c_y(v)] - \ddot{c}_y(v)[c_x(u) - c_x(v)]\Big\}\right). \tag{A.5}$$

Subsequently, we can have the normal vector ${}^{\mathrm{i}}N$ of the tangent plane T_pS:

$$\begin{aligned} {}^{\mathrm{i}}N &= S_{,u} \times S_{,u} \\ &= \sqrt{-{}^{\mathrm{i}}K} \cdot \left[\frac{\dot{c}_x(u)\dot{c}_y(v) - \dot{c}_y(u)\dot{c}_x(v)}{4} \right] \\ &\quad \cdot \left(\frac{-c_y(u) + c_y(v)}{2}, \ \frac{c_x(u) - c_x(v)}{2}, \ \frac{1}{\sqrt{-{}^{\mathrm{i}}K}} \right). \end{aligned} \tag{A.6}$$

The dual surface S^{δ} of surface (eq. 11 has the first derivatives:

$$\begin{aligned} S^{\delta}_{,u} = \sqrt{-{}^{\mathrm{i}}K} \cdot \Bigg(& \frac{\dot{c}_y(u)}{2}, \ \frac{-\dot{c}_x(u)}{2}, \\ & - \dot{c}_x(u)[c_y(u) + c_y(v)] + \dot{c}_y(u)[c_x(u) + c_x(v)] \Bigg), \end{aligned} \tag{A.7}$$

$$\begin{aligned} S^{\delta}_{,v} = \sqrt{-{}^{\mathrm{i}}K} \cdot \Bigg(& \frac{-\dot{c}_y(v)}{2}, \ \frac{\dot{c}_x(v)}{2}, \\ & \dot{c}_x(v)[c_y(u) + c_y(v)] - \dot{c}_y(v)[c_x(u) + c_x(v)] \Bigg). \end{aligned} \tag{A.8}$$